.

TOPOLOGY OPTIMIZATION OF INCOMPRESSIBLE STRUCTURES SUBJECT TO FLUID-STRUCTURE INTERACTION

INOCENCIO CASTAÑAR[§], JOAN BAIGES[*,§] AND RAMON CODINA[§,‡]

Abstract. *In this work, an algorithm for topology optimization of incompressible structures is proposed, in both small and finite strain assumptions and in which the loads come from the interaction with a surrounding fluid. The algorithm considers a classical block-iterative scheme, in which the solid and the fluid mechanics problems are solved sequentially to simulate the interaction between them. Several stabilized mixed finite element formulations based on the Variational Multi-Scale approach are considered to be capable of tackling the incompressible limit for the numerical approximation of the solid. The fluid is considered as an incompressible Newtonian fluid flow which is combined with an Arbitrary-Lagrangian Eulerian formulation to account for the moving part of the domain. Several numerical examples are presented and discussed to assess the robustness of the proposed algorithm and its applicability to the topology optimization of incompressible elastic solids subjected to Newtonian incompressible fluid loads.*

Keywords: Fluid-Structure Interaction (FSI); Topology Optimization (TO); Stabilized finite element methods; Mixed formulations; Incompressible elasticity; Orthogonal SubGrid Scales (OSGS)

Contents

Date: October 10, 2024.

* Corresponding author. E-mail: `joan.baiges@upc.edu` (JB).

§ Universitat Politècnica de Catalunya, Barcelona Tech, Jordi Girona 1-3, Edifici C1, 08034 Barcelona, Spain.

‡ Centre Internacional de Mètodes Numèrics en Enginyeria (CIMNE), Edifici C1, Campus Nord UPC, Gran Capitán S/N, 08034 Barcelona, Spain.

E-mails: `inocencio.castanar@upc.edu` (IC), `ramon.codina@upc.edu` (RC).

1. Introduction

Fluid-Structure Interaction (FSI) problems involve the interaction between a fluid and a deformable solid structure. These problems arise in various engineering and scientific applications, including aerospace [1], civil engineering [2], biomechanics [3, 4], and offshore structures [5]. Numerical methods play a significant role in solving FSI problems by providing efficient and accurate solutions. These methods combine fluid dynamics and structural mechanics algorithms to simulate the coupled behavior of fluids and structures. The interaction between the fluid and the structure is typically modeled by exchanging information at the fluid-structure interface [6]. Understanding and accurately simulating FSI phenomena is crucial for designing and optimizing systems where fluid and structure interact [7, 8].

One common approach for simulating FSI problems is the partitioned approach, where separate solvers are used for the fluid and structural domains. In this approach, the fluid solver calculates the fluid flow field while treating the structure as a rigid body or prescribing its motion based on the interaction forces. The structural solver computes the deformation and stress response of the solid structure based on the fluid-induced loads. The coupling between the two solvers is achieved by iteratively exchanging information at the fluid-structure interface until convergence is reached [9, 10].

FSI problems involving incompressible structures are a subset of FSI phenomena where the solid component undergoes negligible volume changes when subjected to external forces or deformations. In such problems, the fluid interacts with a solid object that remains essentially incompressible, maintaining its volume throughout the interaction [11]. The study of FSI involving incompressible solids is crucial in numerous fields, including biomechanics, bioengineering, soft robotics, and material science [12, 13]. Examples of incompressible structures include soft tissues, elastomers, gels, and certain biological materials [14, 15, 16]. Understanding the complex interactions between the fluid and the incompressible solid is essential for designing and optimizing systems in these domains.

Mixed formulations are commonly used in the context of incompressible structures to handle the incompressibility constraint. These formulations introduce additional unknowns, such as the pressure field, to enforce volume conservation. The most widely used mixed formulations are the displacement-pressure mixed formulations [17, 18] or the three-field formulations which add some extra unknowns to increase its accuracy [19, 20, 21]. These formulations provide stable and accurate solutions for incompressible problems by coupling the displacement and pressure fields; in this work, they are employed to model FSI simulations involving incompressible structures.

Topology Optimization (TO) is a powerful computational design approach that aims to optimize the material distribution within a given design domain to achieve desired performance objectives. The goal is to find the optimal arrangement or layout of material that meets specified criteria while considering design constraints [22]. The primary objective of TO of incompressible structures is to improve structural stiffness while ensuring volume conservation. In these problems, the incompressibility constraint needs to be satisfied throughout the optimization process, meaning that the total volume or the fraction of occupied material within the design domain remains constant [23, 24].

TO is an efficient method to improve mechanical systems design in engineering. In the last decades, several methods have been developed to find optimal structures inside predefined design domains by minimizing objective functions and constraints [22, 25, 26, 27, 28]. In [29] the TO of incompressible structures is studied by considering stabilized mixed formulations and using the topological derivative (TD) concept. It is observed that

the optimal topology for structural elements in the incompressible limit can significantly differ from that of compressible or slightly compressible ones. The TO of hyperelastic materials is also studied in [30, 31] with the combination of a level-set method and the well-known SIMP approach.

Although the field of structural optimization has become mature, many applications, such as aeronautics or biomechanics, require multiphysics design [32, 33, 34, 35, 36]. As a consequence, methodologies for structural TO in FSI problems have become popular as they provide a framework to include FSI models in the TO design procedure.

These methodologies are classified in [37] according to the treatment applied on the interface between the fluid flow and the structure. Therefore, those cases in which only the internal part of the structure is optimized are named "dry" or design-independent optimization, whereas the "wet" or design-dependent optimization are those cases in which the geometry of the FSI boundary can be changed during the TO process.

Regarding the latter, several methodologies have been proposed during the last years. In [38] the idea of using a monolithic approach to interpolate both structural and fluid equations based on the density method was proposed for steady-state FSI problems. These ideas were lately extended to stress-based TO [39]. Another option was proposed in [40] to extend the XFEM-Level-set method reported in [37] to "wet" optimization. The bi-directional evolutionary structural optimization is also applied in [41] to disjoint the problem into two subdomains and be able to tackle them in a separate way. A body-fitted mesh evolution technique integrated into a level-set method can be found in [42]. Finally, reaction-diffusion equation-based level-set methods are applied to solve the FSI optimization problem presented in [43]. All these works concern the interaction between a linear elastic compressible structure and viscous fluid flows governed by the incompressible Navier-Stokes equations. In [44] the TO of structures subject to stationary FSI is adressed.

In this work, we are interested in "dry" TO for FSI problems which may involve incompressible structures. In particular, FSI problems which are two-way coupled. The flow depends on the structural displacements and the structural behavior depends upon the fluid forces. As the FSI boundary remains constant over the TO procedure, we can use a staggered approach to solve individually the fluid and the structure sub-problems and satisfy the interface conditions in a strongly coupled manner [9].

In this study, we propose a new "dry" TO framework for strongly-coupled FSI systems with incompressible structures. To the best of our knowledge, this is the first attempt to use TD-based TO of incompressible structures in FSI problems. Furthermore, the structural model can be either linear elastic or hyperelastic, allowing for finite strain deformations. In addition, the study of transient FSI problems is also performed.

This work is organized as follows. In Section 2 some preliminaries are introduced. Next, in Section 3 we present several stabilized mixed formulations which are able to tackle the incompressible limit to model solid dynamics in both linear elasticity and finite strain hyperelasticity. Section 4 provides the governing equations to deal with incompressible fluid flows with moving domains. Afterwards, Section 5 outlines the setting of the whole TO problem of incompressible structures subjected to FSI loads. Several numerical examples are shown in Section 6 to assess and validate the proposed methodology. The work is closed with some conclusions in Section 7.

2. Preliminaries

This section provides a foundational introduction to the key concepts, theories, methodologies and background knowledge necessary for understanding the main content for all sub-problems presented in this work.

Let us introduce some notation for deriving the weak formulation of the problems we need to develop. As usual, the space of square integrable functions in a domain ω is denoted by

$L^2(\omega)$, whereas the space of functions whose first derivative is square integrable is denoted by $H^1(\omega)$. The space $H_0^1(\omega)$ consists of functions in $H^1(\omega)$ vanishing on boundaries. We shall use the symbol $(\cdot,\cdot)_\omega$ to refer to the $L^2(\omega)$ inner product and $\langle\cdot,\cdot\rangle_\omega$ to refer to the integral of the product of two functions in a domain ω, not necessarily in $L^2(\omega)$. The subscript is omitted when $\omega=\Omega$, being Ω the domain of study for each sub-problem.

For the sake of conciseness, in this work only the implicit second order backward differences scheme (BDF2) is considered. Let us now consider a partition of the time interval $[0,T]$ into N time steps of size δt, assumed to be constant. Given a generic time dependent function at a time step $t^{n+1}=t^n+\delta t$, for $n=0,1,2,\dots$, the approximation of both the first and the second time derivatives of second order are written using information from already computed time instants and f^{n+1} which is being computed at this time step according to the following approximation:

$$\left.\frac{\delta_2 f}{\delta t}\right|_{t^{n+1}} := \frac{3f^{n+1}-4f^n+f^{n-1}}{2\delta t} = \left.\frac{\partial f}{\partial t}\right|_{t^{n+1}} + \mathcal{O}(\delta t^2),$$

$$\left.\frac{\delta_2^2 f}{\delta t^2}\right|_{t^{n+1}} := \frac{2f^{n+1}-5f^n+4f^{n-1}-f^{n-2}}{\delta t^2} = \left.\frac{\partial^2 f}{\partial t^2}\right|_{t^{n+1}} + \mathcal{O}(\delta t^2).$$

Appropriate initializations are required for $n=1,2$.

For all formulations, the standard Galerkin approximation is considered as follows. Let $\mathcal{P}_h$ denote a finite element (FE) partition of the domain of study Ω. The diameter of an element domain $K\in\mathcal{P}_h$ is denoted by h_K and the diameter on the FE partition by $h=\max\{h_K|K\in\mathcal{P}_h\}$. We can now construct conforming FE spaces $\mathbb{X}_h\subset\mathbb{X}$ being $\mathbb{X}$ any proper functional space where an unknown solution is well-defined, as well as the corresponding subspace $\mathbb{X}_{h,0}\subset\mathbb{X}_0$, $\mathbb{X}_0$ being made with functions that vanish on the Dirichlet boundary.

Furthermore, all the formulations used in this work must be stabilized so as to avoid satisfying inf-sup conditions among the unknowns of the problem and to tackle the incompressible limit (see, e.g., [45]). The stabilized FE method we propose to use in the following is based on the Variational Multi-Scale (VMS) concept [46, 47]. Let $\mathbb{X}=\mathbb{X}_h\oplus\tilde{\mathbb{X}}$, where $\tilde{\mathbb{X}}$ is any space to complete $\mathbb{X}_h$ in $\mathbb{X}$. The elements of this space are denoted by $\tilde{\mathbf{X}}$ and they are called subgrid scales (SGSs). Likewise, let $\mathbb{X}_0=\mathbb{X}_{h,0}\oplus\tilde{\mathbb{X}}_0$. In this work, we consider Orthogonal SubGrid Scales (OSGS), where the SGS space is considered to be orthogonal to the FE space, as it is argued in [48]. Furthermore, a key property of the OSGS stabilization is that, thanks to the projection onto the FE space, we keep the consistency of the formulation in a weak sense in spite of including just the minimum number of terms to stabilize the solution [49, 50], allowing us to define a term-by-term stabilization technique called Split OSGS (S-OSGS), which is the one we consider in this work.

3. Solid dynamics problem

This section focuses on the analysis and behavior of solid structures that can reach the incompressible limit under dynamic loading conditions. It explores the response of materials and structures. Let us start by summarizing the conservation equations for both linear elasticity and finite strain hyperelasticity in solid dynamics.

3.1. **Mixed formulations in linear elasticity.**

3.1.1. *The continuum problem.* In this section, the equations of motion of an elastic body under the linear theory of elasticity are considered. Let the solid domain $\Omega_{\mathrm{s}}(t)$ be an open, bounded and polyhedral domain of $\mathbb{R}^d$, where d is the number of space dimensions. Any point of the body is labeled with the vector $\mathbf{x}$. The boundary of the domain is denoted as $\Gamma_{\mathrm{s}}(t):=\partial\Omega_{\mathrm{s}}(t)$. We denote as $]0,T[$ the time interval of analysis for all problems to be

considered. Let $\mathfrak{D}_\mathrm{s} = \{(\mathbf{x},t)|\ \mathbf{x} \in \Omega_\mathrm{s}(t), 0 < t < T\}$ be the space-time domain where the solid problem is defined.

The continuum problem for solid dynamics, suitable for reaching the incompressible limit, is defined by the following system of equations:

$$\rho_\mathrm{s}\frac{\partial^2 \mathbf{u}_\mathrm{s}}{\partial t^2} - \nabla\cdot\mathbf{s}_\mathrm{s} + \nabla p_\mathrm{s} = \rho_\mathrm{s}\mathbf{b} \qquad \text{in } \Omega_\mathrm{s}(t), t \in]0,T[, \tag{1}$$

$$\mathbf{s}_\mathrm{s} - \mathbb{C}^\mathrm{dev} : \mathbf{e}_\mathrm{s} = \mathbf{0} \qquad \text{in } \Omega_\mathrm{s}(t), t \in]0,T[, \tag{2}$$

$$\nabla\cdot\mathbf{u}_\mathrm{s} + \frac{p_\mathrm{s}}{\kappa_\mathrm{s}} = 0 \qquad \text{in } \Omega_\mathrm{s}(t), t \in]0,T[, \tag{3}$$

$$\mathbf{e}_\mathrm{s} - \mathbb{D} : \nabla^\mathrm{s}\mathbf{u}_\mathrm{s} = \mathbf{0} \qquad \text{in } \Omega_\mathrm{s}(t), t \in]0,T[, \tag{4}$$

$$\mathbf{u}_\mathrm{s} = \mathbf{u}_{\mathrm{s},D} \qquad \text{on } \Gamma_{\mathrm{s},D}, t \in]0,T[, \tag{5}$$

$$\mathbf{n}_\mathrm{s}\cdot\mathbf{s}_\mathrm{s} - p_\mathrm{s}\mathbf{n}_\mathrm{s} = \mathbf{t}_{\mathrm{s},N} \qquad \text{on } \Gamma_{\mathrm{s},N}, t \in]0,T[, \tag{6}$$

$$\mathbf{n}_\mathrm{i}\cdot\mathbf{s}_\mathrm{s} - p_\mathrm{s}\mathbf{n}_\mathrm{i} = \mathbf{t}_\mathrm{f} \qquad \text{on } \Gamma_\mathrm{i}(t), t \in]0,T[, \tag{7}$$

$$\mathbf{u}_\mathrm{s} = \mathbf{u}_\mathrm{s}^0 \qquad \text{in } \Omega_\mathrm{s}(0), t = 0, \tag{8}$$

$$\frac{\partial \mathbf{u}_\mathrm{s}}{\partial t} \coloneqq \mathbf{v}_\mathrm{s} = \mathbf{v}_\mathrm{s}^0 \qquad \text{in } \Omega_\mathrm{s}(0), t = 0, \tag{9}$$

where $\mathbf{u}_\mathrm{s}$ is the displacement field, $\mathbf{s}_\mathrm{s}$ the deviatoric stress field, p_s the pressure field and $\mathbf{e}_\mathrm{s}$ the deviatoric strain field. Eq. (1) is the balance of momentum equation, where ρ_s is the density field and $\rho_\mathrm{s}\mathbf{b}$ represents the external load per unit of volume. Here, $\nabla\cdot(\cdot)$ is the divergence operator and $\nabla(\cdot)$ is the gradient operator. Eq. (2) is the deviatoric constitutive equation, where $\mathbb{C}^\mathrm{dev}$ is the 4th order deviatoric constitutive tensor, which for isotropic materials is defined as

$$\mathbb{C}^\mathrm{dev} = 2\mu_\mathrm{s}\left\{\mathbb{I} - \frac{1}{3}\mathbf{I}\otimes\mathbf{I}\right\} \coloneqq 2\mu_\mathrm{s}\mathbb{D}.$$

Here, $\mathbb{I}$ and $\mathbf{I}$ are the 4th and 2nd rank identity tensors, respectively, $\mathbb{D}$ the 4th order deviatoric operator and $\mu_\mathrm{s} = \frac{E_\mathrm{s}}{2(1+\nu_\mathrm{s})}$ the shear modulus, being E_s the Young modulus and ν_s the Poisson ratio. Eq. (3) is the volumetric constitutive equation which imposes the incompressibility constraint, where $\kappa_\mathrm{s} = \frac{E_\mathrm{s}}{3(1-2\nu_\mathrm{s})}$ is the bulk modulus. Finally, Eq. (4) is the deviatoric kinematic equation which relates the deviatoric strain field with the displacement field, where $\nabla^\mathrm{s}(\cdot)$ denotes the symmetric gradient operator.

A set of boundary conditions is considered which can be split into Dirichlet boundary conditions (5), where prescribed displacements $\mathbf{u}_{\mathrm{s},D}$ are specified, Neumann boundary conditions (6) where a prescribed value for the tractions $\mathbf{t}_{\mathrm{s},N}$ are applied, and the transmission conditions on the interface boundary (7), where $\mathbf{t}_\mathrm{f}$ are the tractions coming from the surrounding fluid (the continuity of velocities will be assigned as transmission condition to the flow problem). Vector $\mathbf{n}_\mathrm{s}$ is the geometric unit outward normal vector on the boundary $\Gamma_\mathrm{s}(t)$ and $\mathbf{n}_\mathrm{i}$ the unit normal pointing from the fluid side to the solid one on the interface boundary. The governing equations must be supplied with initial conditions for displacements (8) and velocities (9) in $\Omega_\mathrm{s}(0)$, with $\mathbf{u}_\mathrm{s}^0$ and $\mathbf{v}_\mathrm{s}^0$ given.

Two different mixed formulations are considered in this subsection. On the one hand, the well-known **u**-p formulation, which is introduced in order to deal with nearly and fully incompressible scenarios [17]. On the other hand, the **u**-p-**e** formulation, which includes the **u**-p formulation to tackle the incompressible limit and introduces deviatoric strains to obtain a higher accuracy in the computation of both stresses and strains [51, 19, 20]. Both formulations are explained in detail in [29].

3.1.2. *The* **u**-p *formulation.* The first formulation we consider is the well-known mixed **u**-p formulation, which is introduced to deal with nearly and fully incompressible materials.

The problem consists of finding both a displacement $\mathbf{u}_\mathrm{s} : \mathfrak{D}_\mathrm{s} \to \mathbb{R}^d$ and a pressure $p_\mathrm{s} : \mathfrak{D}_\mathrm{s} \to \mathbb{R}$ such that

$$\rho_\mathrm{s}\frac{\partial^2 \mathbf{u}_\mathrm{s}}{\partial t^2} - \nabla\cdot\left\{\mathbb{C}^\mathrm{dev} : \nabla^\mathrm{s}\mathbf{u}_\mathrm{s}\right\} + \nabla p_\mathrm{s} = \rho_\mathrm{s}\mathbf{b} \qquad \text{in } \Omega_\mathrm{s}(t), t\in\,]0,T[\,, \tag{10}$$

$$\nabla\cdot\mathbf{u}_\mathrm{s} + \frac{p_\mathrm{s}}{\kappa_\mathrm{s}} = 0 \qquad \text{in } \Omega_\mathrm{s}(t), t\in\,]0,T[\,. \tag{11}$$

The problem must be supplied with the already-defined boundary and initial conditions.

Let $\mathbb{U} = \left[H^1(\Omega_\mathrm{s})\right]^d$ and $\mathbb{P} = L^2(\Omega_\mathrm{s})$ be, respectively, the proper functional spaces where displacement and pressure solutions are well-defined. We denote by $\mathbb{U}_0$ functions in $\mathbb{U}$ which vanish on the Dirichlet boundary $\Gamma_{\mathrm{s},D}$. We shall be interested also in the spaces $\mathbb{W} \coloneqq \mathbb{U}\times\mathbb{P}$ and $\mathbb{W}_0 \coloneqq \mathbb{U}_0 \times \mathbb{P}$. The variational statement of the problem is derived by testing the system presented in Eqs. (10-11) against arbitrary test functions $\breve{\mathbf{U}}_\mathrm{s} \coloneqq [\breve{\mathbf{u}}_\mathrm{s}, \breve{p}_\mathrm{s}]^T$, $\breve{\mathbf{u}}_\mathrm{s} \in \mathbb{U}_0$ and $\breve{p}_\mathrm{s} \in \mathbb{P}$. The weak form of the problem reads: find $\mathbf{U}_\mathrm{s} \coloneqq [\mathbf{u}_\mathrm{s}, p_\mathrm{s}]^T :]0,T[\to \mathbb{W}$ such that initial and Dirichlet boundary conditions are satisfied and

$$\left\langle \rho_\mathrm{s}\frac{\partial^2\mathbf{u}_\mathrm{s}}{\partial t^2}, \breve{\mathbf{u}}_\mathrm{s}\right\rangle + \mathcal{A}\left(\mathbf{U}_\mathrm{s}, \breve{\mathbf{U}}_\mathrm{s}\right) = \mathcal{F}\left(\breve{\mathbf{U}}_\mathrm{s}\right) \quad \forall \breve{\mathbf{U}}_\mathrm{s} \in \mathbb{W}_0,$$

where $\mathcal{A}\left(\mathbf{U}_\mathrm{s}, \breve{\mathbf{U}}_\mathrm{s}\right)$ is a bilinear form defined on $\mathbb{W}\times\mathbb{W}_0$ as

$$\mathcal{A}\left(\mathbf{U}_\mathrm{s}, \breve{\mathbf{U}}_\mathrm{s}\right) \coloneqq \left(\mathbb{C}^\mathrm{dev} : \nabla^s\mathbf{u}_\mathrm{s}, \nabla^s\breve{\mathbf{u}}_\mathrm{s}\right) - \left(p_\mathrm{s}, \nabla\cdot\breve{\mathbf{u}}_\mathrm{s}\right) + \left(\nabla\cdot\mathbf{u}_\mathrm{s}, \breve{p}_\mathrm{s}\right) + \left(\frac{1}{\kappa_\mathrm{s}}p_\mathrm{s}, \breve{p}_\mathrm{s}\right),$$

and $\mathcal{F}\left(\breve{\mathbf{U}}_\mathrm{s}\right)$ is a linear form defined on $\mathbb{W}_0$ as

$$\mathcal{F}\left(\breve{\mathbf{U}}_\mathrm{s}\right) \coloneqq \langle\rho_\mathrm{s}\mathbf{b}, \breve{\mathbf{u}}_\mathrm{s}\rangle + \langle\mathbf{t}_{\mathrm{s},N}, \breve{\mathbf{u}}_\mathrm{s}\rangle_{\Gamma_{\mathrm{s},N}} - \langle\mathbf{t}_\mathrm{f}, \breve{\mathbf{u}}_\mathrm{s}\rangle_{\Gamma_\mathrm{i}}.$$

The VMS stabilized $\mathbf{u}$-p formulation of the problem for a discrete Galerkin approximation and with a BDF2 time discretization reads: find $\mathbf{U}_{\mathrm{s},h} \coloneqq [\mathbf{u}_{\mathrm{s},h}, p_{\mathrm{s},h}]^T :]0,T[\to \mathbb{W}_h$ such that initial and Dirichlet boundary conditions are satisfied and

$$\begin{aligned}\left\langle \rho_\mathrm{s}\frac{\delta_2^2\mathbf{u}_{\mathrm{s},h}}{\delta t^2}, \breve{\mathbf{u}}_{\mathrm{s},h}\right\rangle + &\mathcal{A}\left(\mathbf{U}_{\mathrm{s},h}, \breve{\mathbf{U}}_{\mathrm{s},h}\right) + \sum_K \tau_\mathbf{u}\left\langle \Pi_h^\perp\left(\nabla p_{\mathrm{s},h}\right), \nabla\breve{p}_{\mathrm{s},h}\right\rangle_K \\ &+ \sum_K \tau_p\left\langle \Pi_h^\perp\left(\nabla\cdot\mathbf{u}_{\mathrm{s},h}\right), \nabla\cdot\breve{\mathbf{u}}_{\mathrm{s},h}\right\rangle_K = \mathcal{F}\left(\breve{\mathbf{U}}_{\mathrm{s},h}\right) \quad \forall\breve{\mathbf{U}}_{\mathrm{s},h} \in \mathbb{W}_{h,0},\end{aligned}$$

where $\Pi_h^\perp$ is the $L^2(\Omega_\mathrm{s})$ projection onto the orthogonal FE space and $\tau_\mathbf{u}$ and τ_p are coefficients coming from a Fourier analysis of the problem for the SGSs. In this work, we use the stabilization parameters proposed in [51] for linear elastic cases

$$\tau_\mathbf{u} = c_1\frac{h_K^2}{2\mu_\mathrm{s}} \quad \text{and} \quad \tau_p = 2c_2\mu_\mathrm{s},$$

where $c_1 = 4$ and $c_2 = 2$ are the algorithmic parameters used in the numerical examples (using linear elements). Note that it is possible to write the formulation in a symmetric form by applying $\Pi_h^\perp$ also to the operators acting on the test functions.

3.1.3. *The* $\mathbf{u}$-p-$\mathbf{e}$ *formulation.* In this subsection we present the mixed three-field formulation used to deal with the solid dynamics problem. We introduce the mixed $\mathbf{u}$-p-$\mathbf{e}$ problem, which consists of finding a displacement field $\mathbf{u}_\mathrm{s} : \mathfrak{D}_\mathrm{s} \to \mathbb{R}^d$, a pressure $p_\mathrm{s} : \mathfrak{D}_\mathrm{s} \to \mathbb{R}$ and a deviatoric strain field $\mathbf{e}_\mathrm{s} : \mathfrak{D}_\mathrm{s} \to \mathbb{R}^d \otimes \mathbb{R}^d$ such that

$$\rho_\mathrm{s}\frac{\partial^2\mathbf{u}_\mathrm{s}}{\partial t^2} - \nabla\cdot\left\{\mathbb{C}^\mathrm{dev} : \mathbf{e}_\mathrm{s}\right\} + \nabla p_\mathrm{s} = \rho_\mathrm{s}\mathbf{b} \qquad \text{in } \Omega_\mathrm{s}(t), t\in\,]0,T[\,, \tag{12}$$

$$\nabla\cdot\mathbf{u}_\mathrm{s} + \frac{p_\mathrm{s}}{\kappa_\mathrm{s}} = 0 \qquad \text{in } \Omega_\mathrm{s}(t), t\in\,]0,T[\,, \tag{13}$$

$$2\mu_{\mathrm{s}}\mathbf{e}_{\mathrm{s}} - \mathbb{C}^{\mathrm{dev}} : \nabla^{\mathrm{s}}\mathbf{u}_{\mathrm{s}} = 0 \qquad \text{in } \Omega_{\mathrm{s}}(t), t \in]0,T[\,. \tag{14}$$

The governing equations must be supplied with the already-defined boundary and initial conditions.

Let us consider the same spaces and test functions we have defined previously for the mixed $\mathbf{u}$-p formulation. Let also $\mathbb{E} = \left[L^2(\Omega_{\mathrm{s}})\right]^{d\times d}$ be the proper functional space where deviatoric strain components are well-defined. We shall be interested also in the spaces $\mathbb{W} \coloneqq \mathbb{U}\times\mathbb{P}\times\mathbb{E}$ and $\mathbb{W}_0 \coloneqq \mathbb{U}_0\times\mathbb{P}\times\mathbb{E}$. The variational statement of the problem is derived by testing system (12-14) against arbitrary test functions $\breve{\mathbf{U}}_{\mathrm{s}} \coloneqq [\breve{\mathbf{u}}_{\mathrm{s}}, \breve{p}_{\mathrm{s}}, \breve{\mathbf{e}}_{\mathrm{s}}]^T$, $\breve{\mathbf{e}}_{\mathrm{s}} \in \mathbb{E}$. The weak form of the problem reads: find $\mathbf{U}_{\mathrm{s}} \coloneqq [\mathbf{u}_{\mathrm{s}}, p_{\mathrm{s}}, \mathbf{e}_{\mathrm{s}}]^T :]0,T[\to \mathbb{W}$ such that initial and Dirichlet boundary conditions are satisfied and

$$\left\langle \rho_{\mathrm{s}}\frac{\partial^2\mathbf{u}_{\mathrm{s}}}{\partial t^2}, \breve{\mathbf{u}}_{\mathrm{s}} \right\rangle + \mathcal{A}\left(\mathbf{U}_{\mathrm{s}}, \breve{\mathbf{U}}_{\mathrm{s}}\right) = \mathcal{F}\left(\breve{\mathbf{U}}_{\mathrm{s}}\right) \quad \forall \breve{\mathbf{U}}_{\mathrm{s}} \in \mathbb{W}_0,$$

where $\mathcal{A}\left(\mathbf{U}_{\mathrm{s}}, \breve{\mathbf{U}}_{\mathrm{s}}\right)$ is a bilinear form defined on $\mathbb{W}\times\mathbb{W}_0$ as

$$\begin{aligned}\mathcal{A}\left(\mathbf{U}_{\mathrm{s}}, \breve{\mathbf{U}}_{\mathrm{s}}\right) \coloneqq &\left(\mathbb{C}^{\mathrm{dev}} : \mathbf{e}_{\mathrm{s}}, \nabla^s\breve{\mathbf{u}}_{\mathrm{s}}\right) - \left(p_{\mathrm{s}}, \nabla\cdot\breve{\mathbf{u}}_{\mathrm{s}}\right) + \left(\nabla\cdot\mathbf{u}_{\mathrm{s}}, \breve{p}_{\mathrm{s}}\right)\\ &+ \left(\frac{1}{\kappa_{\mathrm{s}}}p_{\mathrm{s}}, \breve{p}_{\mathrm{s}}\right) - \left(\nabla^s\mathbf{u}_{\mathrm{s}}, \mathbb{C}^{\mathrm{dev}} : \breve{\mathbf{e}}_{\mathrm{s}}\right) + \left(2\mu_{\mathrm{s}}\mathbf{e}_{\mathrm{s}}, \breve{\mathbf{e}}_{\mathrm{s}}\right),\end{aligned}$$

and $\mathcal{F}\left(\breve{\mathbf{U}}_{\mathrm{s}}\right)$ is the same linear form as the one defined for the $\mathbf{u}$-p formulation. To avoid overloading the notation, we shall always use $\mathcal{A}$ to denote the form that defines the problem, regardless of the formulation employed.

The VMS stabilized $\mathbf{u}$-p-$\mathbf{e}$ formulation of the problem for a discrete Galerkin approximation and with a BDF2 time discretization reads: find $\mathbf{U}_{\mathrm{s},h} \coloneqq [\mathbf{u}_{\mathrm{s},h}, p_{\mathrm{s},h}, \mathbf{e}_{\mathrm{s},h}]^T :]0,T[\to \mathbb{W}$ such that initial and Dirichlet boundary conditions are satisfied and

$$\begin{aligned}\left\langle \rho_{\mathrm{s}}\frac{\delta_2^2\mathbf{u}_{\mathrm{s},h}}{\delta t^2}, \breve{\mathbf{u}}_{\mathrm{s},h} \right\rangle &+ \mathcal{A}\left(\mathbf{U}_{\mathrm{s},h}, \breve{\mathbf{U}}_{\mathrm{s},h}\right) + \sum_K \tau_{\mathbf{u}}\left\langle \Pi_h^{\perp}\left(\nabla p_{\mathrm{s},h}\right), \nabla\breve{p}_{\mathrm{s},h}\right\rangle_K\\ &+ \sum_K \tau_p\left\langle \Pi_h^{\perp}\left(\nabla\cdot\mathbf{u}_{\mathrm{s},h}\right), \nabla\cdot\breve{\mathbf{u}}_{\mathrm{s},h}\right\rangle_K\\ &+ \sum_K \tau_{\mathbf{e}}\left\langle \Pi_h^{\perp}\left(\mathbb{D} : \nabla^{\mathrm{s}}\mathbf{u}_{\mathrm{s},h}\right), \mathbb{C}^{\mathrm{dev}} : \nabla^s\breve{\mathbf{u}}_{\mathrm{s},h}\right\rangle_K = \mathcal{F}\left(\breve{\mathbf{U}}_{\mathrm{s},h}\right) \quad \forall\breve{\mathbf{U}}_{\mathrm{s},h} \in \mathbb{W}_{h,0},\end{aligned}$$

where $\tau_{\mathbf{e}} = c_3$, being $c_3 = 0.1$ the algorithmic parameter used in the numerical examples.

3.2. **Mixed formulations in finite strain hyperelasticity.** In this subsection the equations of motion of an elastic body under the finite strain theory of hyperelasticity are presented in a total Lagrangian formulation framework. We employ the super index zero for quantities acting at the reference configuration. Let $\Omega_{\mathrm{s}}^0 \coloneqq \Omega_{\mathrm{s}}(0)$ be the reference configuration of the solid body, whereas the current configuration of the body at time t is denoted by $\Omega_{\mathrm{s}}(t)$. The motion is described by a function $\boldsymbol{\psi}$ which links a material particle $\mathbf{X} \in \Omega_{\mathrm{s}}^0$ to the spatial configuration $\mathbf{x} \in \Omega_{\mathrm{s}}(t)$ according to

$$\boldsymbol{\psi} : \Omega_{\mathrm{s}}^0 \longrightarrow \Omega_{\mathrm{s}}(t), \quad \mathbf{x} = \boldsymbol{\psi}(\mathbf{X}, t), \quad \forall\mathbf{X} \in \Omega_{\mathrm{s}}^0, \quad t \geq 0.$$

The boundary of the reference configuration is denoted as $\Gamma_{\mathrm{s}}^0 \coloneqq \partial\Omega_{\mathrm{s}}^0$. The interface boundary with the fluid at the reference configuration is $\Gamma_{\mathrm{i}}^0 \coloneqq \Gamma_{\mathrm{i}}(0)$. Let now $\mathfrak{D}_{\mathrm{s}} = \left\{(\mathbf{X}, t) |\ \mathbf{X} \in \Omega_{\mathrm{s}}^0, 0 < t < T\right\}$ be the space-time domain where the solid problem is defined. All the spatial derivatives are understood to be taken with respect to the material coordinates $\mathbf{X}$.

We want to deal with compressible materials that can reach the incompressible limit. The governing equations in finite strain hyperelasticity are:

$$\rho_{\mathrm{s}}^0 \frac{\partial^2 \mathbf{u}_{\mathrm{s}}}{\partial t^2} - \nabla \cdot \left\{ \mathbf{S}'_{\mathrm{s}} \mathbf{F}_{\mathrm{s}}^T \right\} + \nabla \cdot \left\{ p_{\mathrm{s}} J_{\mathrm{s}} \mathbf{F}_{\mathrm{s}}^{-1} \right\} = \rho_{\mathrm{s}}^0 \mathbf{b} \qquad \text{in } \Omega_{\mathrm{s}}^0, t \in]0,T[\,, \tag{15}$$

$$\frac{p_{\mathrm{s}}}{\kappa_{\mathrm{s}}} + \frac{dG_{\mathrm{s}}}{dJ_{\mathrm{s}}} = 0 \qquad \text{in } \Omega_{\mathrm{s}}^0, t \in]0,T[\,, \tag{16}$$

$$\mathbf{S}'_{\mathrm{s}} - 2\frac{\partial W_{\mathrm{s}}}{\partial \mathbf{C}_{\mathrm{s}}} = \mathbf{0} \qquad \text{in } \Omega_{\mathrm{s}}^0, t \in]0,T[\,, \tag{17}$$

$$\mathbf{u}_{\mathrm{s}} = \mathbf{u}_{\mathrm{s},D} \qquad \text{on } \Gamma_{\mathrm{s},D}^0, t \in]0,T[\,, \tag{18}$$

$$\mathbf{N}_{\mathrm{s}} \cdot \left\{ \mathbf{S}'_{\mathrm{s}} \mathbf{F}_{\mathrm{s}}^T - p_{\mathrm{s}} J_{\mathrm{s}} \mathbf{F}_{\mathrm{s}}^{-1} \right\} = \mathbf{T}_{\mathrm{s},N} \qquad \text{on } \Gamma_{\mathrm{s},N}^0, t \in]0,T[\,, \tag{19}$$

$$\mathbf{N}_{\mathrm{i}} \cdot \left\{ \mathbf{S}'_{\mathrm{s}} \mathbf{F}_{\mathrm{s}}^T - p_{\mathrm{s}} J_{\mathrm{s}} \mathbf{F}_{\mathrm{s}}^{-1} \right\} = J_{\mathrm{s}} \mathbf{F}_{\mathrm{s}}^{-1} \mathbf{t}_{\mathrm{f}} \qquad \text{on } \Gamma_{\mathrm{i}}^0, t \in]0,T[\,, \tag{20}$$

$$\mathbf{u}_{\mathrm{s}} = \mathbf{u}_{\mathrm{s}}^0 \qquad \text{in } \Omega_{\mathrm{s}}^0, t = 0, \tag{21}$$

$$\mathbf{v}_{\mathrm{s}} = \mathbf{v}_{\mathrm{s}}^0 \qquad \text{in } \Omega_{\mathrm{s}}^0, t = 0, \tag{22}$$

where $\mathbf{S}'_{\mathrm{s}}$ is the deviatoric second Piola Kirchhoff (PK2) stress tensor and p_{s} the pressure field. Eq. (15) is the balance of momentum equation, where $\mathbf{F}_{\mathrm{s}} = \frac{\partial \mathbf{x}}{\partial \mathbf{X}}$ is the deformation gradient and $J_{\mathrm{s}} = \det \mathbf{F}_{\mathrm{s}} > 0$ is the Jacobian of the deformation. Eq. (16) is the volumetric constitutive equation, which imposes the incompressibility constraint when $\kappa_{\mathrm{s}} \to \infty$, and where G_{s} is a function which depends on the volumetric part of the strain energy model. In this work, we select the Simo-Taylor law [52], which is defined as

$$G_{\mathrm{s}}(J_{\mathrm{s}}) = \frac{1}{4}\left(J_{\mathrm{s}}^2 - 1 - 2\,\log\,J_{\mathrm{s}}\right), \quad \frac{dG_{\mathrm{s}}}{dJ_{\mathrm{s}}} = \frac{1}{2}\left(J_{\mathrm{s}} - \frac{1}{J_{\mathrm{s}}}\right).$$

Finally, Eq. (17) is the deviatoric constitutive equation, which allows us to relate the displacement field with the deviatoric PK2 stress tensor through the deviatoric part of the strain energy function W_{s}. In this work, we restrict ourselves to a neo-Hookean material model [53], which is defined as

$$W_{\mathrm{s}}(\mathbf{C}_{\mathrm{s}}) = \frac{\mu_{\mathrm{s}}}{2}\left(J_{\mathrm{s}}^{-\frac{2}{3}}\mathrm{tr}\ \mathbf{C}_{\mathrm{s}} - 3\right), \quad \frac{\partial W_{\mathrm{s}}}{\partial \mathbf{C}_{\mathrm{s}}} = \frac{\mu_{\mathrm{s}}}{2} J_{\mathrm{s}}^{-\frac{2}{3}}\left\{\mathbf{I} - \frac{1}{3}(\mathrm{tr}\ \mathbf{C}_{\mathrm{s}})\mathbf{C}_{\mathrm{s}}^{-1}\right\},$$

where $\mathbf{C}_{\mathrm{s}} = \mathbf{F}_{\mathrm{s}}^T \mathbf{F}_{\mathrm{s}}$ is the right Cauchy-Green tensor and $\mathrm{tr}\ \mathbf{C}_{\mathrm{s}} = \mathbf{C}_{\mathrm{s}} : \mathbf{I}$ is the trace of $\mathbf{C}_{\mathrm{s}}$.

With regards to the boundary conditions (18-20), $\mathbf{u}_{\mathrm{s},D}$ is a prescribed value for the displacements on the Dirichlet boundary, $\mathbf{T}_{\mathrm{s},N}$ a prescribed value for the tractions on the Neumann boundary and $\mathbf{t}_{\mathrm{f}}$ are the tractions coming from the fluid on the interface boundary. Note that a pull-back transformation must be applied to fluid tractions $\mathbf{t}_{\mathrm{f}}$ to apply them on the boundaries at the reference configuration. Vector $\mathbf{N}_{\mathrm{s}}$ is the geometric unit outward normal vector on the boundary Γ_{s}^0 and $\mathbf{N}_{\mathrm{i}}$ the unit normal pointing from the fluid side to the solid one on the interface boundary at the reference configuration. The governing equations must be supplied with initial conditions for displacements (21) and velocities (22) in Ω_{s}^0, with $\mathbf{u}_{\mathrm{s}}^0$ and $\mathbf{v}_{\mathrm{s}}^0$ given.

As for the linear case, two different mixed formulations are considered to manage this problem. On the one hand, the mixed two-field $\mathbf{u}$-p formulation presented in [18], in which the addition of the pressure field as an extra primary variable with respect to the classical displacement-based formulation is considered to be able to enforce the incompressibility constraint. On the other hand, a novel mixed three-field $\mathbf{u}$-p-$\mathbf{S}'$ formulation which is presented in [21], in which the deviatoric PK2 stress tensor is added as unknown of the problem. The final goal is to design a FE technology able to tackle simultaneously problems which may involve incompressible behavior together with a high degree of accuracy of the stress field.

3.2.1. *The* **u**-p *formulation.* The first formulation we consider is the mixed two-field **u**-p formulation, which is introduced to deal with nearly and fully incompressible materials. The problem consists of finding both a displacement $\mathbf{u}_\mathrm{s} : \mathfrak{D}_\mathrm{s} \to \mathbb{R}^d$ and a pressure $p_\mathrm{s} : \mathfrak{D}_\mathrm{s} \to \mathbb{R}$ such that

$$\rho_\mathrm{s}^0 \frac{\partial^2 \mathbf{u}_\mathrm{s}}{\partial t^2} - \nabla \cdot \left\{ \mathbf{S}_\mathrm{s}' \mathbf{F}_\mathrm{s}^T \right\} + \nabla \cdot \left\{ p_\mathrm{s} J_\mathrm{s} \mathbf{F}_\mathrm{s}^{-1} \right\} = \rho_\mathrm{s}^0 \mathbf{b} \qquad \text{in } \Omega_\mathrm{s}^0, t \in]0,T[\,, \tag{23}$$

$$\frac{p_\mathrm{s}}{\kappa_\mathrm{s}} + \frac{dG_\mathrm{s}}{dJ_\mathrm{s}} = 0 \qquad \text{in } \Omega_\mathrm{s}^0, t \in]0,T[\,, \tag{24}$$

where $\mathbf{S}_\mathrm{s}'$, $\mathbf{F}_\mathrm{s}$, J_s and $\frac{dG_\mathrm{s}}{dJ_\mathrm{s}}$ are functions of the displacement field. The problem must be supplied with the already-defined boundary and initial conditions.

Let $\mathbb{U}$ and $\mathbb{P}$ be, respectively, the proper functional spaces where displacement and pressure solutions are well-defined. We denote by $\mathbb{U}_0$ functions in $\mathbb{U}$ which vanish on the Dirichlet boundary $\Gamma_{\mathrm{s},D}^0$. We shall be interested also in the spaces $\mathbb{W} \coloneqq \mathbb{U} \times \mathbb{P}$ and $\mathbb{W}_0 \coloneqq \mathbb{U}_0 \times \mathbb{P}$. The variational statement of the problem is derived by testing the system presented in Eqs. (23-24) against arbitrary test functions $\breve{\mathbf{U}}_\mathrm{s} \coloneqq [\breve{\mathbf{u}}_\mathrm{s}, \breve{p}_\mathrm{s}]^T$, $\breve{\mathbf{u}}_\mathrm{s} \in \mathbb{U}_0$ and $\breve{p}_\mathrm{s} \in \mathbb{P}$. The weak form of the problem reads: find $\mathbf{U}_\mathrm{s} \coloneqq [\mathbf{u}_\mathrm{s}, p_\mathrm{s}]^T :]0,T[\to \mathbb{W}$ such that initial and Dirichlet boundary conditions are satisfied and

$$\left\langle \rho_\mathrm{s}^0 \frac{\partial^2 \mathbf{u}_\mathrm{s}}{\partial t^2}, \breve{\mathbf{u}}_\mathrm{s} \right\rangle + \mathcal{A}\left(\mathbf{U}_\mathrm{s}, \breve{\mathbf{U}}_\mathrm{s}\right) = \mathcal{F}\left(\breve{\mathbf{U}}_\mathrm{s}\right) \quad \forall \breve{\mathbf{U}}_\mathrm{s} \in \mathbb{W}_0,$$

where $\mathcal{A}\left(\mathbf{U}_\mathrm{s}, \breve{\mathbf{U}}_\mathrm{s}\right)$ is a semi-linear form defined on $\mathbb{W} \times \mathbb{W}_0$ as

$$\mathcal{A}\left(\mathbf{U}_\mathrm{s}, \breve{\mathbf{U}}_\mathrm{s}\right) \coloneqq \left\langle \mathbf{S}_\mathrm{s}' \mathbf{F}_\mathrm{s}^T, \nabla \breve{\mathbf{u}}_\mathrm{s} \right\rangle - \left\langle p_\mathrm{s} J_\mathrm{s} \mathbf{F}_\mathrm{s}^{-1}, \nabla \breve{\mathbf{u}}_\mathrm{s} \right\rangle + \left\langle \frac{dG_\mathrm{s}}{dJ_\mathrm{s}}, \breve{p}_\mathrm{s} \right\rangle + \left\langle \frac{p_\mathrm{s}}{\kappa_\mathrm{s}}, \breve{p}_\mathrm{s} \right\rangle,$$

and $\mathcal{F}\left(\breve{\mathbf{U}}_\mathrm{s}\right)$ is a linear form defined on $\mathbb{W}_0$ as

$$\mathcal{F}\left(\breve{\mathbf{U}}_\mathrm{s}\right) \coloneqq \left\langle \rho_\mathrm{s}^0 \mathbf{b}, \breve{\mathbf{u}}_\mathrm{s} \right\rangle + \left\langle \mathbf{T}_{\mathrm{s},N}, \breve{\mathbf{u}}_\mathrm{s} \right\rangle_{\Gamma_{\mathrm{s},N}^0} - \left\langle J_\mathrm{s} \mathbf{F}_\mathrm{s}^{-1} \mathbf{t}_\mathrm{f}, \breve{\mathbf{u}}_\mathrm{s} \right\rangle_{\Gamma_\mathrm{i}^0}.$$

In order to solve the problem, the system needs to be linearized, so that a bilinear operator which allows to compute a correction $\delta\mathbf{U}_\mathrm{s}$ of a given guess for the solution at time t^{n+1} is obtained, that we denote by $\mathbf{U}_\mathrm{s}$. Iteration counters will be omitted to simplify the notation. After using a Newton-Raphson scheme, we obtain the following linearized form of the problem. Given $\mathbf{U}_\mathrm{s}$ as the solution at time t^{n+1} and the previous iteration, find a correction $\delta\mathbf{U}_\mathrm{s} \coloneqq [\delta\mathbf{u}_\mathrm{s}, \delta p_\mathrm{s}]^T :]0,T[\to \mathbb{W}_0$ such that

$$\left\langle \rho_\mathrm{s}^0 \frac{\partial^2 \mathbf{u}_\mathrm{s}}{\partial t^2}, \breve{\mathbf{u}}_\mathrm{s} \right\rangle + \mathcal{B}\left(\delta\mathbf{U}_\mathrm{s}, \breve{\mathbf{U}}_\mathrm{s}\right) = \mathcal{F}\left(\breve{\mathbf{U}}_\mathrm{s}\right) - \mathcal{A}\left(\mathbf{U}_\mathrm{s}, \breve{\mathbf{U}}_\mathrm{s}\right) \quad \forall \breve{\mathbf{U}}_\mathrm{s} \in \mathbb{W}_0,$$

where $\mathcal{B}\left(\delta\mathbf{U}_\mathrm{s}, \breve{\mathbf{U}}_\mathrm{s}\right)$ is the bilinear form obtained through a Newton-Raphson linearization and it is defined on $\mathbb{W}_0 \times \mathbb{W}_0$ as

$$\begin{aligned}
\mathcal{B}\left(\delta\mathbf{U}_\mathrm{s}, \breve{\mathbf{U}}_\mathrm{s}\right) = {} & \left\langle \nabla\delta\mathbf{u}_\mathrm{s} \mathbf{S}_\mathrm{s}', \nabla\breve{\mathbf{u}}_\mathrm{s} \right\rangle + \left\langle \mathbb{C}' : \left\{ \mathbf{F}_\mathrm{s} \nabla\delta\mathbf{u}_\mathrm{s} \right\}, \left\{ \mathbf{F}_\mathrm{s} \nabla\breve{\mathbf{u}}_\mathrm{s} \right\}^T \right\rangle \\
& - \left\langle J_\mathrm{s} p_\mathrm{s} \left\{ \nabla\delta\mathbf{u}_\mathrm{s} : \mathbf{F}_\mathrm{s}^{-T} \right\} \mathbf{F}_\mathrm{s}^{-1}, \nabla\breve{\mathbf{u}}_\mathrm{s} \right\rangle + \left\langle J_\mathrm{s} p_\mathrm{s} \left\{ \mathbf{F}_\mathrm{s}^{-1} \nabla\delta\mathbf{u}_\mathrm{s} \right\}, \left\{ \mathbf{F}_\mathrm{s}^{-1} \nabla\breve{\mathbf{u}}_\mathrm{s} \right\}^T \right\rangle \\
& - \left\langle J_\mathrm{s} \delta p_\mathrm{s} \mathbf{F}_\mathrm{s}^{-1}, \nabla\breve{\mathbf{u}}_\mathrm{s} \right\rangle + \left\langle f_\mathrm{s}(J_\mathrm{s}) \left\{ \nabla\delta\mathbf{u}_\mathrm{s} : \mathbf{F}_\mathrm{s}^{-T} \right\}, \breve{p}_\mathrm{s} \right\rangle + \left\langle \frac{\delta p_\mathrm{s}}{\kappa_\mathrm{s}}, \breve{p}_\mathrm{s} \right\rangle,
\end{aligned}$$

where $f_\mathrm{s}(J_\mathrm{s})$ is a function coming from the linearization of $\frac{dG_\mathrm{s}}{dJ_\mathrm{s}}$ and $\mathbb{C}'$ is the deviatoric constitutive tangent matrix; these terms are:

$$f_\mathrm{s}(J_\mathrm{s}) = \frac{1}{2}\left(J_\mathrm{s} + \frac{1}{J_\mathrm{s}}\right),$$

$$\mathbb{C}' = 4\frac{\partial^2 W_{\rm s}}{\partial \mathbf{C}_{\rm s}\partial \mathbf{C}_{\rm s}} = \frac{2\mu_{\rm s}}{3} J_{\rm s}^{-\frac{2}{3}} \left\{ \frac{1}{3}(\text{tr } \mathbf{C}_{\rm s})\mathbf{C}_{\rm s}^{-1}\otimes\mathbf{C}_{\rm s}^{-1} - (\text{tr } \mathbf{C}_{\rm s})\frac{\partial \mathbf{C}_{\rm s}^{-1}}{\partial \mathbf{C}_{\rm s}} - \mathbf{C}_{\rm s}^{-1}\otimes\mathbf{I} - \mathbf{I}\otimes\mathbf{C}_{\rm s}^{-1} \right\}.$$

The VMS stabilized $\mathbf{u}$-p formulation of the linearized problem for a discrete Galerkin approximation and with a BDF2 time discretization is given by

$$\left\langle \rho_{\rm s}^0 \frac{\delta_2^2 \mathbf{u}_{{\rm s},h}}{\delta t^2}, \breve{\mathbf{u}}_{{\rm s},h} \right\rangle + \mathcal{B}\left(\delta\mathbf{U}_{{\rm s},h}, \breve{\mathbf{U}}_{{\rm s},h}\right) + \sum_K \tau_{\mathbf{u}} \left\langle \mathfrak{B}(\delta\mathbf{U}_{{\rm s},h}), \mathfrak{L}(\breve{\mathbf{U}}_{{\rm s},h}) \right\rangle_K$$
$$= \mathcal{F}\left(\breve{\mathbf{U}}_{{\rm s},h}\right) - \mathcal{A}\left(\mathbf{U}_{{\rm s},h}, \breve{\mathbf{U}}_{{\rm s},h}\right) - \sum_K \tau_{\mathbf{u}} \left\langle \Pi_h^{\perp}\left(\mathfrak{A}(\mathbf{U}_{{\rm s},h})\right), \mathfrak{L}(\breve{\mathbf{U}}_{{\rm s},h}) \right\rangle_K \quad \forall \breve{\mathbf{U}}_{{\rm s},h} \in \mathbb{W}_{h,0},$$

where

$$\mathfrak{L}(\breve{\mathbf{U}}_{{\rm s},h}) = -f_{\rm s}(J_{{\rm s},h})\nabla \breve{p}_{{\rm s},h}\mathbf{F}_{{\rm s},h}^{-1},$$
$$\mathfrak{A}\left(\mathbf{U}_{{\rm s},h}\right) = -J_{{\rm s},h}\nabla p_{{\rm s},h}\mathbf{F}_{{\rm s},h}^{-1},$$
$$\mathfrak{B}(\delta\mathbf{U}_{{\rm s},h}) = -J_{{\rm s},h}\left\{\nabla\delta\mathbf{u}_{{\rm s},h} : \mathbf{F}_{{\rm s},h}^{-T}\right\}\nabla p_{{\rm s},h}\mathbf{F}_{{\rm s},h}^{-1} + J_{{\rm s},h}\nabla p_{{\rm s},h}\mathbf{F}_{{\rm s},h}^{-1}\nabla\delta\mathbf{u}_{{\rm s},h}\mathbf{F}_{{\rm s},h}^{-1} - J_{{\rm s},h}\nabla\delta p_{{\rm s},h}\mathbf{F}_{{\rm s},h}^{-1},$$

$\Pi_h^{\perp}$ is the $L^2(\Omega_{\rm s}^0)$ projection onto the orthogonal FE space and $\tau_{\mathbf{u}}$ is defined in [18] as

$$\tau_{\mathbf{u}} = c_1 \frac{h_K^2}{2\mu_{\rm s}},$$

where $c_1 = 1.0$ is the algorithmic parameter applied in the numerical examples (using linear elements).

3.2.2. *The* $\mathbf{u}$-p-$\mathbf{S}'$ *formulation.* In this subsection we present the mixed three-field formulation used to deal with the solid dynamics problem. It consists of finding a displacement field $\mathbf{u}_{\rm s} : \mathfrak{D}_{\rm s} \to \mathbb{R}^d$, a pressure $p_{\rm s} : \mathfrak{D}_{\rm s} \to \mathbb{R}$ and a deviatoric PK2 stress field $\mathbf{S}'_{\rm s} : \mathfrak{D}_{\rm s} \to \mathbb{R}^d \otimes \mathbb{R}^d$ such that

$$\rho_{\rm s}^0 \frac{\partial^2 \mathbf{u}_{\rm s}}{\partial t^2} - \nabla\cdot\left\{\mathbf{S}'_{\rm s}\mathbf{F}_{\rm s}^T\right\} + \nabla\cdot\left\{p_{\rm s}J_{\rm s}\mathbf{F}_{\rm s}^{-1}\right\} = \rho_{\rm s}^0\mathbf{b} \qquad \text{in } \Omega_{\rm s}^0, t\in\,]0,T[\,, \tag{25}$$

$$\frac{p_{\rm s}}{\kappa_{\rm s}} + \frac{dG_{\rm s}}{dJ_{\rm s}} = 0 \qquad \text{in } \Omega_{\rm s}^0, t\in\,]0,T[\,, \tag{26}$$

$$\mathbf{S}'_{\rm s} - 2\frac{\partial W_{\rm s}}{\partial \mathbf{C}_{\rm s}} = \mathbf{0} \qquad \text{in } \Omega_{\rm s}^0, t\in\,]0,T[\,, \tag{27}$$

where $\mathbf{F}_{\rm s}$, $J_{\rm s}$, $\frac{dG_{\rm s}}{dJ_{\rm s}}$ and $\frac{\partial W_{\rm s}}{\partial \mathbf{C}_{\rm s}}$ are functions of the displacement field. The problem must be supplied with the already-defined boundary and initial conditions. Note that tensor $\mathbf{S}'_{\rm s}$ is in fact *not* deviatoric, but it comes from the volumetric-deviatoric splitting of the Cauchy stress tensor.

Let us consider the same spaces and test functions we have defined previously for the mixed $\mathbf{u}$-p formulation. Let $\mathbb{S}$ be the proper functional space where the deviatoric PK2 stress components are well-defined. We shall be interested also in the spaces $\mathbb{W} \coloneqq \mathbb{U}\times\mathbb{P}\times\mathbb{S}$ and $\mathbb{W}_0 \coloneqq \mathbb{U}_0\times\mathbb{P}\times\mathbb{S}$. The variational statement of the problem is derived by testing system (25-27) against arbitrary test functions $\breve{\mathbf{U}}_{\rm s} \coloneqq \left[\breve{\mathbf{u}}_{\rm s}, \breve{p}_{\rm s}, \breve{\mathbf{S}}'\right]^T$, $\breve{\mathbf{S}}' \in \mathbb{S}$. The weak form of the problem reads: find $\mathbf{U}_{\rm s} \coloneqq [\mathbf{u}_{\rm s}, p_{\rm s}, \mathbf{S}'_{\rm s}]^T :]0,T[\to \mathbb{W}$ such that initial and Dirichlet boundary conditions are satisfied and

$$\left\langle \rho_{\rm s}^0 \frac{\partial^2 \mathbf{u}_{\rm s}}{\partial t^2}, \breve{\mathbf{u}}_{\rm s} \right\rangle + \mathcal{A}\left(\mathbf{U}_{\rm s}, \breve{\mathbf{U}}_{\rm s}\right) = \mathcal{F}\left(\breve{\mathbf{U}}_{\rm s}\right) \quad \forall \breve{\mathbf{U}}_{\rm s} \in \mathbb{W}_0,$$

where $\mathcal{A}\left(\mathbf{U}_{\rm s}, \breve{\mathbf{U}}_{\rm s}\right)$ is a semi-linear form defined on $\mathbb{W}\times\mathbb{W}_0$ as

$$\mathcal{A}\left(\mathbf{U}_{\rm s}, \breve{\mathbf{U}}_{\rm s}\right) \coloneqq \left\langle \mathbf{S}'_{\rm s}\mathbf{F}_{\rm s}^T, \nabla\breve{\mathbf{u}}_{\rm s}\right\rangle - \left\langle p_{\rm s}J_{\rm s}\mathbf{F}_{\rm s}^{-1}, \nabla\breve{\mathbf{u}}_{\rm s}\right\rangle + \left\langle \frac{dG_{\rm s}}{dJ_{\rm s}}, \breve{p}_{\rm s}\right\rangle$$

$$+\left\langle \frac{p_{\mathrm{s}}}{\kappa_{\mathrm{s}}},\breve{p}_{\mathrm{s}}\right\rangle -\left\langle 2\frac{\partial W_{\mathrm{s}}}{\partial\mathbf{C}_{\mathrm{s}}},\breve{\mathbf{S}}'\right\rangle +\left\langle \mathbf{S}'_{\mathrm{s}},\breve{\mathbf{S}}'\right\rangle ,$$

and $\mathcal{F}\left(\breve{\mathbf{U}}_{\mathrm{s}}\right)$ is the same linear form as the one defined for the $\mathbf{u}$-p formulation.

After using a Newton-Raphson scheme, we obtain the following linearized form of the problem. Given $\mathbf{U}_{\mathrm{s}}$ as the solution at time t^{n+1} and the previous iteration, find a correction $\delta\mathbf{U}_{\mathrm{s}}\coloneqq[\delta\mathbf{u}_{\mathrm{s}},\delta p_{\mathrm{s}},\delta\mathbf{S}'_{\mathrm{s}}]^{T}:]0,T[\to\mathbb{W}_{0}$ such that

$$\left\langle \rho_{\mathrm{s}}^{0}\frac{\partial^{2}\mathbf{u}_{\mathrm{s}}}{\partial t^{2}},\breve{\mathbf{u}}_{\mathrm{s}}\right\rangle +\mathcal{B}\left(\delta\mathbf{U}_{\mathrm{s}},\breve{\mathbf{U}}_{\mathrm{s}}\right)=\mathcal{F}\left(\breve{\mathbf{U}}_{\mathrm{s}}\right)-\mathcal{A}\left(\mathbf{U}_{\mathrm{s}},\breve{\mathbf{U}}_{\mathrm{s}}\right)\quad\forall\breve{\mathbf{U}}_{\mathrm{s}}\in\mathbb{W}_{0},$$

where $\mathcal{B}\left(\delta\mathbf{U}_{\mathrm{s}},\breve{\mathbf{U}}_{\mathrm{s}}\right)$ is a bilinear form defined on $\mathbb{W}_{0}\times\mathbb{W}_{0}$ as

$$\begin{aligned}\mathcal{B}\left(\delta\mathbf{U}_{\mathrm{s}},\breve{\mathbf{U}}_{\mathrm{s}}\right)&=\left\langle \nabla\delta\mathbf{u}_{\mathrm{s}}\mathbf{S}'_{\mathrm{s}},\nabla\breve{\mathbf{u}}_{\mathrm{s}}\right\rangle +\left\langle \mathbf{F}_{\mathrm{s}}\delta\mathbf{S}'_{\mathrm{s}},\nabla\breve{\mathbf{u}}_{\mathrm{s}}\right\rangle -\left\langle J_{\mathrm{s}}p_{\mathrm{s}}\left\{\mathbf{F}_{\mathrm{s}}^{-1}:\nabla\delta\mathbf{u}_{\mathrm{s}}\right\}\mathbf{F}_{\mathrm{s}}^{-1},\nabla\breve{\mathbf{u}}_{\mathrm{s}}\right\rangle \\&+\left\langle J_{\mathrm{s}}p_{\mathrm{s}}\left\{\mathbf{F}_{\mathrm{s}}^{-1}\nabla\delta\mathbf{u}_{\mathrm{s}}\right\},\left\{\mathbf{F}_{\mathrm{s}}^{-1}\nabla\breve{\mathbf{u}}_{\mathrm{s}}\right\}^{T}\right\rangle -\left\langle J_{\mathrm{s}}\delta p_{\mathrm{s}}\mathbf{F}_{\mathrm{s}}^{-1},\nabla\breve{\mathbf{u}}_{\mathrm{s}}\right\rangle \\&+\left\langle f_{\mathrm{s}}(J_{\mathrm{s}})\left\{\mathbf{F}_{\mathrm{s}}^{-1}:\nabla\delta\mathbf{u}_{\mathrm{s}}\right\},\breve{p}_{\mathrm{s}}\right\rangle +\left\langle \frac{\delta p_{\mathrm{s}}}{\kappa_{\mathrm{s}}},\breve{p}_{\mathrm{s}}\right\rangle -\left\langle \mathbb{C}':\left\{\mathbf{F}_{\mathrm{s}}\nabla\delta\mathbf{u}_{\mathrm{s}}\right\},\breve{\mathbf{S}}'\right\rangle +\left\langle \delta\mathbf{S}'_{\mathrm{s}},\breve{\mathbf{S}}'\right\rangle ,\end{aligned}$$

The VMS stabilized $\mathbf{u}$-p-$\mathbf{S}'$ formulation of the linearized problem for a discrete Galerkin approximation and with a BDF2 time discretization is given by:

$$\begin{aligned}&\left\langle \rho_{\mathrm{s}}^{0}\frac{\delta_{2}^{2}\mathbf{u}_{\mathrm{s},h}}{\delta t^{2}},\breve{\mathbf{u}}_{\mathrm{s},h}\right\rangle +\mathcal{B}\left(\delta\mathbf{U}_{\mathrm{s},h},\breve{\mathbf{U}}_{\mathrm{s},h}\right)+\sum_{K}\tau_{\mathbf{u}}\left\langle \mathfrak{B}_{\mathbf{u}}(\delta\mathbf{U}_{\mathrm{s},h}),\mathfrak{L}_{\mathbf{u}}(\breve{\mathbf{U}}_{\mathrm{s},h})\right\rangle _{K}\\&\qquad+\sum_{K}\tau_{\mathbf{S}'}\left\langle \mathfrak{B}_{\mathbf{S}'}(\delta\mathbf{U}_{\mathrm{s},h}),\mathfrak{L}_{\mathbf{S}'}(\breve{\mathbf{U}}_{\mathrm{s},h})\right\rangle _{K}=\mathcal{F}\left(\breve{\mathbf{U}}_{\mathrm{s},h}\right)-\mathcal{A}\left(\mathbf{U}_{\mathrm{s},h},\breve{\mathbf{U}}_{\mathrm{s},h}\right)\\&\qquad-\sum_{K}\tau_{\mathbf{u}}\left\langle \Pi_{h}^{\perp}\left(\mathfrak{A}_{\mathbf{u}}(\mathbf{U}_{\mathrm{s},h})\right),\mathfrak{L}_{\mathbf{u}}(\breve{\mathbf{U}}_{\mathrm{s},h})\right\rangle _{K}-\sum_{K}\tau_{\mathbf{S}'}\left\langle \Pi_{h}^{\perp}\left(\mathfrak{A}_{\mathbf{S}'}(\mathbf{U}_{\mathrm{s},h})\right),\mathfrak{L}_{\mathbf{S}'}(\breve{\mathbf{U}}_{\mathrm{s},h})\right\rangle _{K}\end{aligned}$$

$\forall\breve{\mathbf{U}}_{\mathrm{s},h}\in\mathbb{W}_{h,0}$, where

$$\begin{aligned}\mathfrak{L}_{\mathbf{u}}(\breve{\mathbf{U}}_{\mathrm{s},h})&=-f_{\mathrm{s}}(J_{\mathrm{s},h})\nabla\breve{p}_{\mathrm{s},h}\mathbf{F}_{\mathrm{s},h}^{-1},\quad\mathfrak{L}_{\mathbf{S}'}(\breve{\mathbf{U}}_{\mathrm{s},h})=\left\{\mathbf{F}_{\mathrm{s},h}\nabla\breve{\mathbf{u}}_{\mathrm{s},h}\right\}^{T},\\\mathfrak{A}_{\mathbf{u}}\left(\mathbf{U}_{\mathrm{s},h}\right)&=-J_{\mathrm{s},h}\nabla p_{\mathrm{s},h}\mathbf{F}_{\mathrm{s},h}^{-1},\quad\mathfrak{A}_{\mathbf{S}'}\left(\mathbf{U}_{\mathrm{s},h}\right)=2\frac{\partial W_{\mathrm{s},h}}{\partial\mathbf{C}_{\mathrm{s},h}},\\\mathfrak{B}_{\mathbf{u}}(\delta\mathbf{U}_{\mathrm{s},h})&=-J_{\mathrm{s},h}\left\{\nabla\delta\mathbf{u}_{\mathrm{s},h}:\mathbf{F}_{\mathrm{s},h}^{-T}\right\}\nabla p_{\mathrm{s},h}\mathbf{F}_{\mathrm{s},h}^{-1}+J_{\mathrm{s},h}\nabla p_{\mathrm{s},h}\mathbf{F}_{\mathrm{s},h}^{-1}\nabla\delta\mathbf{u}_{\mathrm{s},h}\mathbf{F}_{\mathrm{s},h}^{-1}-J_{\mathrm{s},h}\nabla\delta p_{\mathrm{s},h}\mathbf{F}_{\mathrm{s},h}^{-1},\\\mathfrak{B}_{\mathbf{S}'}(\delta\mathbf{U}_{\mathrm{s},h})&=\mathbb{C}':\left\{\mathbf{F}_{\mathrm{s},h}\nabla\delta\mathbf{u}_{\mathrm{s},h}\right\},\end{aligned}$$

and $\tau_{\mathbf{S}'}=c_{3}$ is defined as in [21], being $c_{3}=0.5$ the algorithmic parameter applied in the numerical examples.

4. Fluid flow problem

The next step is to define the governing equations that model the flow problem for an incompressible Newtonian fluid, which is modeled with the well-known Navier-Stokes equations. The approach followed can be understood as the traditional one, where the fluid problem is solved by means of an ALE formulation to cope with the time dependency of the fluid domain.

4.1. ALE formulation of the fluid flow equations.

Let $\Omega_{\mathrm{f}}(t)$ be the domain where the fluid flows, with boundary $\Gamma_{\mathrm{f}}(t)\coloneqq\partial\Omega_{\mathrm{f}}(t)$, where Dirichlet boundary conditions are prescribed on $\Gamma_{\mathrm{f},D}(t)$ and Neumann conditions on $\Gamma_{\mathrm{f},N}(t)$. These boundaries may be moving.

Let $\boldsymbol{\chi}_{t}$ be a family of invertible mappings, which for all $t\in[0,T]$ map a point $\mathbf{X}\in\Omega_{\mathrm{f}}(0)$ to a point $\mathbf{x}=\boldsymbol{\chi}_{t}(\mathbf{X})\in\Omega_{\mathrm{f}}(t)$, with $\boldsymbol{\chi}_{0}=\mathbf{I}$, the identity. If $\boldsymbol{\chi}_{t}$ is given by the motion of

the particles, the resulting formulation would be Lagrangian, whereas if $\boldsymbol{\chi}_t = \mathbf{I}$ for all t, $\Omega_{\mathrm{f}}(t) = \Omega_{\mathrm{f}}(0)$ and the formulation would be Eulerian. Let now $t' \in [0,T]$, with $t' \leq t$, and consider the mapping

$$\boldsymbol{\chi}_{t,t'} : \Omega_{\mathrm{f}}(t') \longrightarrow \Omega_{\mathrm{f}}(t), \quad \mathbf{x}' \mapsto \mathbf{x} = \boldsymbol{\chi}_t \circ \boldsymbol{\chi}_{t'}^{-1}(\mathbf{x}').$$

Let $\mathfrak{D}_{\mathrm{f}} = \{(\mathbf{x},t) | \mathbf{x} \in \Omega_{\mathrm{f}}(t),\ 0 < t < T\}$ be the space-time domain where the fluid problem is defined. Given a function $f : \mathfrak{D}_{\mathrm{f}} \longrightarrow \mathbb{R}$ we define

$$\left.\frac{\partial f}{\partial t}\right|_{\mathbf{x}'} (\mathbf{x},t) := \frac{\partial (f \circ \boldsymbol{\chi}_{t,t'})}{\partial t}(\mathbf{x}',t), \quad \mathbf{x} \in \Omega_{\mathrm{f}}(t),\ \mathbf{x}' \in \Omega_{\mathrm{f}}(t').$$

In particular, the domain velocity taking as a reference the coordinates of $\Omega_{\mathrm{f}}(t')$ is given by

$$\mathbf{v}_{\mathrm{dom}} \coloneqq \left.\frac{\partial \mathbf{x}}{\partial t}\right|_{\mathbf{x}'} (\mathbf{x},t).$$

When the flow equations are approximated using the FE method, $\mathbf{v}_{\mathrm{dom}}$ needs to be computed. It is assumed to be given on the boundary $\Gamma_{\mathrm{f}}(t)$. To compute the values for the interior of the domain, a mesh equation must be solved. The mesh equation we use is proposed in [54]. The method considers the mesh as a fictitious linear elastic body subjected to prescribed displacements at the selected moving boundaries. The mechanical properties of each mesh element are appropriately selected in order to minimize the deformation and the distortion of the mesh elements. Let us directly show here the system of equations that is solved for a given velocity field in the interface boundary with the solid domain $\mathbf{v}_{\Gamma_{\mathrm{i}}}$ at time t^n:

$$\begin{aligned} -\nabla \cdot \{\mathbb{C} : \nabla^{\mathrm{s}} \mathbf{v}_{\mathrm{dom}}\} &= \mathbf{0} && \text{in } \Omega_{\mathrm{f}}(t^n), \\ \mathbf{v}_{\mathrm{dom}} &= \mathbf{v}_{\Gamma_{\mathrm{i}}} && \text{on } \Gamma_{\mathrm{i}}(t^n), \\ \mathbf{v}_{\mathrm{dom}} &= \mathbf{0} && \text{on } \Gamma_{\mathrm{f}}(t^n) \setminus \Gamma_{\mathrm{i}}(t^n), \end{aligned}$$

where $\mathbb{C}\left(E_{\mathrm{dom}}\left(\mathbf{x}\right), \nu_{\mathrm{dom}}\right)$ is the constitutive 4th order tensor in linear elasticity, $E_{\mathrm{dom}}\left(\mathbf{x}\right)$ is the Young modulus of the mesh and ν_{dom} is the Poisson coefficient of the mesh.

Using the ALE reference, the only modification with respect to the purely Eulerian formulation is to replace the transport velocity $\mathbf{v}_{\mathrm{f}}$ of the advective term by $\mathbf{v}_{\mathrm{c}} \coloneqq \mathbf{v}_{\mathrm{f}} - \mathbf{v}_{\mathrm{dom}}$. If $\mathbf{v}_{\mathrm{dom}} = \mathbf{0}$ we would recover a purely Eulerian formulation for the fluid.

4.2. **The continuum problem statement.** The equations of the Newtonian incompressible fluid flow assumption are now presented. The continuum Navier-Stokes problem for incompressible Newtonian fluid flows is defined by the following system of equations:

$$\rho_{\mathrm{f}} \frac{\partial \mathbf{v}_{\mathrm{f}}}{\partial t} + \rho_{\mathrm{f}} \mathbf{v}_{\mathrm{c}} \cdot \nabla \mathbf{v}_{\mathrm{f}} - \nabla \cdot \{2\mu_{\mathrm{f}} \nabla^{\mathrm{s}} \mathbf{v}_{\mathrm{f}}\} + \nabla p_{\mathrm{f}} = \mathbf{f} \qquad \text{in } \Omega_{\mathrm{f}}(t), t \in]0,T[\,, \tag{28}$$

$$\nabla \cdot \mathbf{v}_{\mathrm{f}} = 0 \qquad \text{in } \Omega_{\mathrm{f}}(t), t \in]0,T[\,, \tag{29}$$

$$\mathbf{v}_{\mathrm{f}} = \mathbf{v}_{\mathrm{f},D} \qquad \text{on } \Gamma_{\mathrm{f},D}(t), t \in]0,T[\,, \tag{30}$$

$$\mathbf{n}_{\mathrm{f}} \cdot \boldsymbol{\sigma}_{\mathrm{f}} = \mathbf{t}_{\mathrm{f},N} \qquad \text{on } \Gamma_{\mathrm{f},N}(t), t \in]0,T[\,, \tag{31}$$

$$\mathbf{v}_{\mathrm{f}} = \mathbf{v}_{\Gamma_{\mathrm{i}}} \qquad \text{on } \Gamma_{\mathrm{i}}(t), t \in]0,T[\,, \tag{32}$$

$$\mathbf{v}_{\mathrm{f}} = \mathbf{v}_{\mathrm{f}}^0 \qquad \text{in } \Omega_{\mathrm{f}}(0), t = 0, \tag{33}$$

where Eq. (28) is the balance of linear momentum and Eq. (29) the incompressibility constraint. In these equations, $\mathbf{v}_{\mathrm{f}}$ is the velocity field, p_{f} the pressure, $\mathbf{f}$ the vector of body forces, ρ_{f} the density of the fluid and μ_{f} its dynamic viscosity.

With regards to the boundary conditions (30-32), $\mathbf{v}_{\mathrm{f},D}$ is a prescribed value for the velocities on the Dirichlet boundary, $\mathbf{t}_{\mathrm{f},N}$ the prescribed value for the tractions on the Neumann boundary and $\mathbf{v}_{\Gamma_{\mathrm{i}}}$ is the velocity field coming from the solid on the interface

boundary. The governing equations must be supplied with an initial condition for the velocity field (33) in $\Omega_{\mathrm{f}}(0)$, with $\mathbf{v}_{\mathrm{f}}^0$ given.

In this work, the stabilized two-field $\mathbf{v}$-p formulation proposed in [55] is considered. Details can be found in [56]. Here we just write the resulting numerical formulation.

4.3. **The $\mathbf{v}$-p formulation.** In this subsection, the well-known mixed $\mathbf{v}$-p formulation is introduced in order to deal with incompressible Newtonian fluid flows. In the presented formulation the velocity field $\mathbf{v}_{\mathrm{f}} : \mathfrak{D}_{\mathrm{f}} \to \mathbb{R}^d$ and the pressure field $p_{\mathrm{f}} : \mathfrak{D}_{\mathrm{f}} \to \mathbb{R}$ are used as independent variables.

Let $\mathbb{V} = \left[H^1(\Omega_{\mathrm{f}})\right]^d$ and $\mathbb{P} = L^2(\Omega_{\mathrm{f}})$ be, respectively, the proper functional spaces where velocity and pressure solutions are well-defined. We denote by $\mathbb{V}_0$ functions in $\mathbb{V}$ which vanish on the Dirichlet boundary $\Gamma_{\mathrm{f},D}$. We shall be interested also in the spaces $\mathbb{W} \coloneqq \mathbb{V} \times \mathbb{P}$ and $\mathbb{W}_0 \coloneqq \mathbb{V}_0 \times \mathbb{P}$. The variational statement of the problem is derived by testing the system presented in Eqs. (28-29) against arbitrary test functions $\breve{\mathbf{V}}_{\mathrm{f}} \coloneqq [\breve{\mathbf{v}}_{\mathrm{f}}, \breve{p}_{\mathrm{f}}]^T$, $\breve{\mathbf{v}}_{\mathrm{f}} \in \mathbb{V}_0$ and $\breve{p}_{\mathrm{f}} \in \mathbb{P}$. The weak form of the problem reads: find $\mathbf{V}_{\mathrm{f}} \coloneqq [\mathbf{v}_{\mathrm{f}}, p_{\mathrm{f}}]^T :]0,T[\to \mathbb{W}$ such that initial and Dirichlet boundary conditions are satisfied and

$$\left\langle \rho_{\mathrm{f}} \frac{\partial \mathbf{v}_{\mathrm{f}}}{\partial t}, \breve{\mathbf{v}}_{\mathrm{f}} \right\rangle + \mathcal{A}\left(\mathbf{v}_{\mathrm{f}}; \mathbf{V}_{\mathrm{f}}, \breve{\mathbf{V}}_{\mathrm{f}}\right) = \mathcal{F}\left(\breve{\mathbf{V}}_{\mathrm{f}}\right) \quad \forall\ \breve{\mathbf{V}}_{\mathrm{f}} \in \mathbb{W}_0,$$

where, for a fixed $\hat{\mathbf{v}}$, $\mathcal{A}\left(\hat{\mathbf{v}}; \mathbf{V}_{\mathrm{f}}, \breve{\mathbf{V}}_{\mathrm{f}}\right)$ is a bilinear form defined on $\mathbb{W} \times \mathbb{W}_0$ as

$$\mathcal{A}\left(\hat{\mathbf{v}}; \mathbf{V}_{\mathrm{f}}, \breve{\mathbf{V}}_{\mathrm{f}}\right) \coloneqq \langle \rho_{\mathrm{f}} \hat{\mathbf{v}} \cdot \nabla \mathbf{v}_{\mathrm{f}}, \breve{\mathbf{v}}_{\mathrm{f}} \rangle + 2\mu_{\mathrm{f}} \left(\nabla^{\mathrm{s}} \mathbf{v}_{\mathrm{f}}, \nabla \breve{\mathbf{v}}_{\mathrm{f}}\right) - \left(p_{\mathrm{f}}, \nabla \cdot \breve{\mathbf{v}}_{\mathrm{f}}\right) + \left(\nabla \cdot \mathbf{v}_{\mathrm{f}}, \breve{p}_{\mathrm{f}}\right).$$

$\mathcal{F}\left(\breve{\mathbf{V}}_{\mathrm{f}}\right)$ is a linear form defined on $\mathbb{W}_0$ as

$$\mathcal{F}\left(\breve{\mathbf{V}}_{\mathrm{f}}\right) \coloneqq \langle \mathbf{f}, \breve{\mathbf{v}}_{\mathrm{f}} \rangle + \langle \mathbf{t}_{\mathrm{f},N}, \breve{\mathbf{v}}_{\mathrm{f}} \rangle_{\Gamma_{\mathrm{f},N}}.$$

Note that the Navier-Stokes problem to be solved has one source of nonlinearity, namely, the convective term. For the sake of conciseness, we will consider only a fixed-point iterative scheme. In particular, $\hat{\mathbf{v}}$ will be taken as the velocity computed in a previous iteration of a fixed-point scheme.

In this case, we consider the SGSs to be time-dependent; these are solutions of:

$$\begin{aligned}
\rho_{\mathrm{f}} \frac{\partial \tilde{\mathbf{v}}_1}{\partial t} + \tau_{\mathbf{v}}^{-1} \tilde{\mathbf{v}}_1 &= -\Pi_h^{\perp}[\rho_{\mathrm{f}} \mathbf{v}_{\mathrm{c},h} \cdot \nabla \mathbf{v}_{\mathrm{f},h}], \\
\rho_{\mathrm{f}} \frac{\partial \tilde{\mathbf{v}}_2}{\partial t} + \tau_{\mathbf{v}}^{-1} \tilde{\mathbf{v}}_2 &= -\Pi_h^{\perp}[\nabla p_{\mathrm{f},h}], \\
\tilde{p} &= -\tau_p \Pi_h^{\perp}[\nabla \cdot \mathbf{v}_{\mathrm{f},h}],
\end{aligned}$$

where $\tau_{\mathbf{v}}$ and τ_p are coefficients coming from a Fourier analysis of the problem for the SGSs. In this work, we use the stabilization parameters proposed in [56] as

$$\tau_{\mathbf{v}}^{-1} = c_1 \frac{\mu_{\mathrm{f}}}{h_K^2} + c_2 \frac{\rho_{\mathrm{f}} |\hat{\mathbf{v}}_h|}{h_K} \quad \text{and} \quad \tau_p = \tau_{\mathbf{v}}^{-1} h_K^2,$$

where $|\hat{\mathbf{v}}_h|$ is the Euclidean norm of the velocity guess and $c_1 = 4.0$ and $c_2 = 2.0$ are the algorithmic parameters used in the numerical examples using linear elements.

The VMS stabilized $\mathbf{v}$-p formulation of the problem for a discrete Galerkin approximation and with a BDF2 time discretization reads: find $\mathbf{V}_{\mathrm{f},h} \coloneqq [\mathbf{v}_{\mathrm{f},h}, p_{\mathrm{f},h}]^T :]0,T[\to \mathbb{W}_h$ such that initial and Dirichlet boundary conditions are satisfied and

$$\begin{aligned}
\left\langle \rho_{\mathrm{f}} \frac{\delta_2 \mathbf{v}_{\mathrm{f},h}}{\delta t}, \breve{\mathbf{v}}_{\mathrm{f},h} \right\rangle + \mathcal{A}\left(\mathbf{v}_{\mathrm{f},h}; \mathbf{V}_{\mathrm{f},h}, \breve{\mathbf{V}}_{\mathrm{f},h}\right) + \sum_K \langle \tilde{\mathbf{v}}_1, -\rho_{\mathrm{f}} \mathbf{v}_{\mathrm{f},h} \cdot \nabla \breve{\mathbf{v}}_{\mathrm{f},h} \rangle_K + \sum_K \langle \tilde{\mathbf{v}}_2, -\nabla \breve{p}_{\mathrm{f},h} \rangle_K \\
+ \sum_K \langle \tilde{p}, -\nabla \cdot \breve{\mathbf{v}}_{\mathrm{f},h} \rangle_K = \mathcal{F}\left(\breve{\mathbf{V}}_{\mathrm{f},h}\right) \quad \forall\ \breve{\mathbf{V}}_{\mathrm{f},h} \in \mathbb{W}_{h,0}.
\end{aligned}$$

This stabilized ALE formulation for the linear convection-diffusion equation using also BDF2 as time integrator is analyzed in [57]. Let us also remark that if discontinuous pressure interpolations are used (which is not our case), terms involving SGSs on the element boundaries need to be introduced [58].

5. Topology optimization of incompressible structures subject to FSI

5.1. **Fluid-structure interaction.** Let $\Omega(t)$ be the whole domain of the problem, formed by a fluid sub-domain $\Omega_{\mathrm{f}}(t)$ and a solid one $\Omega_{\mathrm{s}}(t)$, which will be optimized during the process. These two sub-domains do not overlap, so that $\bar{\Omega}(t) = \overline{\Omega_{\mathrm{f}}(t) \cup \Omega_{\mathrm{s}}(t)}$ and $\mathring{\Omega}_{\mathrm{f}}(t) \cap \mathring{\Omega}_{\mathrm{s}}(t) = \emptyset$. Recall that the sub-domains have their own boundaries $\Gamma_{\mathrm{f}}(t)$ and $\Gamma_{\mathrm{s}}(t)$, and the interface between them is $\Gamma_{\mathrm{i}}(t)$. Its unit normal with respect to the spatial configuration is denoted as $\mathbf{n}_{\mathrm{i}}$, pointing from the fluid side to the solid one. We also define Γ_{s}^0 as the solid boundary in the reference configuration and its unit normal with respect to the material configuration is denoted by $\mathbf{N}_{\mathrm{i}}$.

In this work, a classical block-iterative coupling is considered, in which the solid and the fluid problems are solved sequentially with a strong coupling. A Dirichlet-Neumann coupling is considered: the solid is solved with the loads computed from the fluid in a given iteration and then the fluid is computed with the velocities on the interface obtained from the solid. To enhance the convergence rate of the coupled solvers, an Aitken relaxation scheme is implemented. By accelerating the convergence, it reduces the number of iterations required to reach a desired level of accuracy, thereby reducing computational time and resources. This is particularly beneficial for complex FSI problems that involve large-scale simulations or real-time applications [9, 59]. Obviously, other iteration-by-subdomain schemes could be used, as those proposed in [60] emanating from the concept of boundary SGSs.

5.2. **Topology optimization of incompressible structures.** In the following, the TO problem is summarized under the assumption of both linear elastic and finite strain hyperelastic isotropic materials. As we are considering a total Lagrangian formulation framework when dealing with finite strain theory, let us use the material coordinates $\mathbf{X}$ and work in the reference configuration for the solid. Obviously, in the linear elastic case we can consider both configurations due to the fact that they are supposed to be very close to each other.

One common objective in TO is minimizing the total potential energy of a structure. The total potential energy is a measure of the internal energy stored within the solid, which is directly related to its stiffness and deformation behavior. By minimizing the potential energy, engineers can design structures that are lightweight yet strong, leading to improved performance and efficiency. In addition to minimizing the potential energy, TO often incorporates volume constraints. These constraints ensure that the resulting optimized design does not exceed a certain volume or mass limit, which is often dictated by practical considerations, such as manufacturing capabilities or weight restrictions. By imposing volume constraints, engineers can ensure that the optimized design remains feasible and practical for real-world applications.

The description of the topology is determined by a characteristic function defined as

$$\chi(\mathbf{X}) = \begin{cases} 1 & \text{if } \mathbf{X} \in \Omega_{\mathrm{str}} \\ 0 & \text{if } \mathbf{X} \in \Omega_{\mathrm{wea}} \end{cases},$$

where the solid domain at the reference configuration Ω_{s}^0 is split into two parts. The sub-domains Ω_{str} and Ω_{wea} are made of different materials. The characteristic function is in charge of determining in the whole domain Ω_{s}^0 what part corresponds to either material.

Such kind of problems are typically termed bi-material TO problems. The material corresponding to the domain Ω_{wea} exhibits a very small stiffness, approximating the absence of material. The material parameters of the strong domain Ω_{str} are denoted by ρ_{str}, E_{str} and ν_{str}, and the parameters of the weak domain Ω_{wea} are taken as $\rho_{\text{wea}} = \gamma\rho_{\text{str}}$, $E_{\text{wea}} = \gamma E_{\text{str}}$, and thus γ stands for the jump of density and stiffness. Note that $\gamma > 0$ is a parameter, small enough to model void regions and large enough to entail invertibility properties to the stiffness matrix. To simplify the problem in the void region, we take the fictitious material there as compressible, i.e., $\nu_{\text{wea}} < 0.5$. This is especially important if the optimization process leads to confined regions of fictitious material, if the material was incompressible there, significant loading could occur in the fictitious region, which would lead to incorrect results (see [29]).

The TO problem is then formulated as the minimization of the total potential energy functional subjected to the material allowed, which is written as follows

$$\begin{aligned} &\min_{\chi\in\mathbb{X}_L} \mathcal{J}(\chi) = \int_{\Omega_{\text{s}}^0} \Psi_{\text{s}}(\chi,\mathbf{X}) - \int_{\Omega_{\text{s}}^0} \rho_{\text{s}}^0 \mathbf{b}\cdot\mathbf{u}_{\text{s}}(\chi,\mathbf{X}) - \int_{\Gamma_{\text{s},N}^0} \mathbf{T}_{\text{s},N}\cdot\mathbf{u}_{\text{s}}(\chi,\mathbf{X}) \\ &\text{s.t. : } \left\langle \rho_{\text{s}}^0 \frac{\partial^2 \mathbf{u}_{\text{s}}}{\partial t^2}, \breve{\mathbf{u}}_{\text{s}} \right\rangle + \mathcal{A}\left(\mathbf{U}_{\text{s}}, \breve{\mathbf{U}}_{\text{s}}\right) = \mathcal{F}\left(\breve{\mathbf{U}}_{\text{s}}\right) \quad \forall \breve{\mathbf{U}}_{\text{s}} \in \mathbb{W}_0, \\ &\mathbb{X}_L = \left\{ \chi \in L^\infty\left(\Omega_{\text{s}}^0, \{0,1\}\right), \int_{\Omega_{\text{s}}^0} \chi(\mathbf{X}) = L|\Omega_{\text{s}}^0| \right\}, \end{aligned} \tag{34}$$

where $\Psi_{\text{s}} = W_{\text{s}} + \kappa_{\text{s}} G_{\text{s}}$ is the strain energy function and $\mathbb{X}_L$ is the feasible domain restricted to a volume constraint denoted as a fraction $0 < L < 1$ of the domain Ω_{s}^0.

Several approaches exist to solve the TO problem (34) for elastic materials. In this work we apply the Topological Derivative (TD) concept [24] together with a level-set approach in order to advance to the optimal topology. The TD is a measurement of the sensitivity of a given functional with respect to the apparition of an infinitesimal inclusion in a given point of the domain of interest.

In the linear elastic case, the TD of this functional at a point $\mathbf{X}$ suitable to reach the incompressible limit can be formally computed according to [29] as

$$\mathcal{D}_T\mathcal{J}(\chi,\mathbf{X}) = \mathbf{e}_{\text{s}}(\chi,\mathbf{X}) : \mathbb{P}^{\text{dev}} : \mathbf{s}_{\text{s}}(\chi,\mathbf{X}) + \mathrm{P}^{\text{vol}} p_{\text{s}}^2(\chi,X) + (1-\gamma)\rho_{\text{s}}^0 \mathbf{b}\cdot\mathbf{u}_{\text{s}}(\chi,\mathbf{X}), \tag{35}$$

where $\mathbb{P}^{\text{dev}}$ and P^{vol} are the deviatoric polarization tensor and the volumetric polarization coefficient, which are defined in [29].

Unfortunately, there is no way to obtain an analytical expression for the TD for finite strain hyperelastic materials. However, an approximation can be found in [61, 62]. In this set of works, the topological sensitivity analysis is applied to finite strain deformation based on the total Lagrangian formulation framework. The numerical study of the asymptotic behavior of the function $\mathcal{D}_T\mathcal{J}(\chi,\mathbf{X})$ with relation to the radius of the hole is developed. It is concluded that the TD of this functional at a point $\mathbf{X}$ can be approximated by

$$\mathcal{D}_T\mathcal{J}(\chi,\mathbf{X}) \approx \mathcal{M}_D\mathcal{J}(\chi,\mathbf{X}) \coloneqq \Psi_{\text{s}}(\chi,\mathbf{X}) + (1-\gamma)\rho_{\text{s}}^0 \mathbf{b}\cdot\mathbf{u}_{\text{s}}(\chi,\mathbf{X}), \tag{36}$$

which is nevertheless expected to be a minimization direction.

Remark 5.1. *Let us discuss some important aspects about the TD approximation we are using when the infinitesimal strain assumption is considered. In such case, the TD approximation is written as*

$$\mathcal{D}_T\mathcal{J}(\chi,\mathbf{X}) \approx \frac{1}{2}\boldsymbol{\varepsilon}_{\text{s}}(\chi,\mathbf{X}) : \boldsymbol{\sigma}_{\text{s}}(\chi,\mathbf{X}) + (1-\gamma)\rho_{\text{s}}^0 \mathbf{b}\cdot\mathbf{u}_{\text{s}}(\chi,\mathbf{X}),$$

where $\boldsymbol{\varepsilon}_{\text{s}}$ is the infinitesimal strain tensor and $\boldsymbol{\sigma}_{\text{s}}$ the Cauchy stress tensor. By comparing this approximation with the analytical TD obtained for linear elastic materials given in [63] *it is seen that these two equations match, if and only if, the polarization tensor $\mathbb{P}$ reduces*

to the 4^{th}-order identity tensor $\mathbb{I}$ (up to constant values, which do not affect the direction of the TD). This only happens when $\nu_s = 0.25$. *Therefore, the TD approximation only matches the exact one when $\nu_s = 0.25$, being just an approximation otherwise. Also in the context of linear elasticity, this approximate TD is justified in* [64] *using the concept of* relaxed *TD. A comparison of this and other approaches can be found in* [65].

We can now define a signed TD such that

$$\overline{\mathcal{D}_T\mathcal{J}}\left(\chi,\mathbf{X}\right)=\begin{cases}-\mathcal{D}_T\mathcal{J}\left(\chi,\mathbf{X}\right) & \text{if } \mathbf{X}\in\Omega_{\text{str}}\\ \mathcal{D}_T\mathcal{J}\left(\chi,\mathbf{X}\right) & \text{if } \mathbf{X}\in\Omega_{\text{wea}}\end{cases}.$$

Let us now introduce the signed TD interpretation. For a given topology, computing the TD allows one to know, for each given material point, how the cost functional would change if the material switches. Once the optimal value for the characteristic function $\chi\left(\mathbf{X}\right)$ is reached, the following condition holds

$$\overline{\mathcal{D}_T\mathcal{J}}\left(\chi,\mathbf{X}\right)\geq\overline{\mathcal{D}_T\mathcal{J}}\left(\chi,\mathbf{Y}\right),\forall\mathbf{X}\in\Omega_{\text{str}},\forall\mathbf{Y}\in\Omega_{\text{wea}}. \tag{37}$$

Note that at the interface $\overline{\Omega_{\text{str}}}\cap\overline{\Omega_{\text{wea}}}$, the TD presents a jump, but the signed TD is continuous. Eq. (37) allows one to construct a level set function, which will implicitly characterize Ω_{str} and Ω_{wea}. This level set function is defined as

$$\psi\left(\chi,\mathbf{X}\right)=\overline{\mathcal{D}_T\mathcal{J}}\left(\chi,\mathbf{X}\right)+\lambda,$$

where $\lambda\in\mathbb{R}$ is a scalar, responsible for ensuring that the volume restriction in Eq. (34) is fulfilled. The level-set function also allows us to characterize the description of the topology:

$$\psi\left(\chi,\mathbf{X}\right)\begin{cases}>0 & \text{if } \mathbf{X}\in\Omega_{\text{str}}\\ <0 & \text{if } \mathbf{X}\in\Omega_{\text{wea}}\end{cases}. \tag{38}$$

Furthermore, the level-set function allows us to keep a sharp interface between materials when $\psi\left(\chi,\mathbf{X}\right)=0$. The scalar λ can be computed by enforcing

$$\int_{\Omega_s^0}H\left(\psi\left(\chi,\mathbf{X}\right)\right)=L|\Omega_s^0|,$$

where H is the Heaviside step function. From Eq. (38), it can be observed that for the solution of Eq. (34) there holds

$$\chi=H\left(\psi\right).$$

We can perform the TO procedure according to the flowchart in Fig 1 (see [66, 29] to see further details on the TO procedure). Let us comment some details about this flowchart.

Initially, the level set function ψ is defined with unit initial value, which means that we consider the structure to be composed of strong material everywhere. Obviously, this first approach does not fulfill the volume constraint. We thus take

$$\psi^0\left(\mathbf{X}\right)=1\quad\text{in }\Omega_s^0.$$

Let ψ^{i-1} be a known level set, where the superscript indicates the TO iteration counter. From this level set value, a characteristic function can be built

$$\chi^i\left(\mathbf{X}\right)=H\left(\psi^{i-1}\left(\mathbf{X}\right)\right)\quad\text{in }\Omega_s^0,$$

which allows one to solve the solid dynamics problem and compute the signed TD. This is independent from the use of any formulation. For convergence aspects, the algorithm also requires an intermediate function $\phi^i\left(\chi^i,\mathbf{X}\right)$. This function is initially defined as the

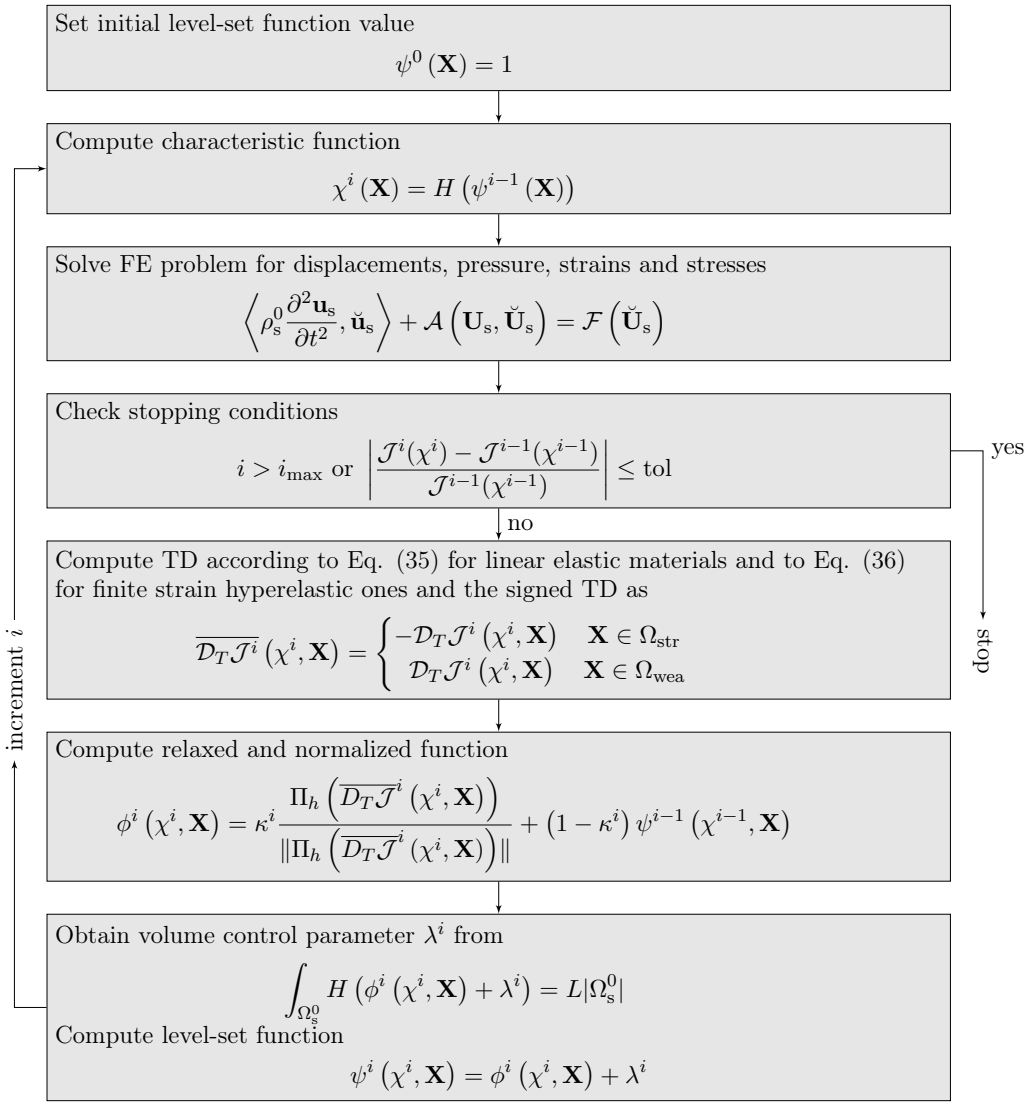

FIGURE 1. Topology optimization algorithm flowchart

projection onto the FE space of the normalized TD in order to bound the level-set function with a relaxation scheme introduced as the iterative process advances, i.e.

$$\phi^i(\chi^i, \mathbf{X}) = \kappa^i \frac{\Pi_h\left(\overline{D_T\mathcal{J}}^i(\chi^i, \mathbf{X})\right)}{\|\Pi_h\left(\overline{D_T\mathcal{J}}^i(\chi^i, \mathbf{X})\right)\|} + (1-\kappa^i)\psi^{i-1}(\chi^{i-1}, \mathbf{X}).$$

The relaxation parameter κ^i is computed according to [66], and Π_h indicates a projection onto the FE space. In the numerical examples, Π_h is computed by using a lumped mass matrix approach for computational efficiency. This approach plays the role of standard filtering in TO. Finally, the level set function at the current iteration is defined as

$$\psi^i(\chi^i, \mathbf{X}) = \phi^i(\chi^i, \mathbf{X}) + \lambda^i,$$

where λ^i is computed by using the secant method to solve the volume constraint equation at iteration i:

$$\int_{\Omega_s^0} H\left(\psi^i(\chi^i, \mathbf{X})\right) = L|\Omega_s^0|.$$

As a stopping criterion we consider the evolution of the objective functional. The algorithm concludes if the functional has not decreased more than a given minimum during a maximum number of iterations. Also, a maximum number of total iterations to be performed is set.

To determine κ^i, a spatial oscillation indicator is computed:

$$\xi^i\left(\chi^i,\mathbf{X}\right)=\text{sign}\left\{\frac{\frac{\Pi_h\left(\overline{D_T\mathcal{J}}^i(\chi^i,\mathbf{X})\right)}{\|\Pi_h\left(\overline{D_T\mathcal{J}}^i(\chi^i,\mathbf{X})\right)\|}-\psi^{i-1}\left(\chi^{i-1},\mathbf{X}\right)}{\psi^{i-1}\left(\chi^{i-1},\mathbf{X}\right)-\psi^{i-2}\left(\chi^{i-2},\mathbf{X}\right)}\right\}.$$

Note that $\xi^i\left(\chi^i,\mathbf{X}\right)=1$ if the iterative algorithm for computing the TD is advancing monotonically in the preceding iterations and $\xi^i\left(\chi^i,\mathbf{X}\right)=-1$ otherwise. This indicator allows one to detect if there are oscillations in the iterative process. If there are oscillations, the value for κ^i needs to be decreased, otherwise it can be increased up to a maximum of 1. An intermediate function $\mu^i\left(\chi^i,\mathbf{X}\right)$ is introduced as

$$\mu^i\left(\chi^i,\mathbf{X}\right)=\begin{cases}k_1\kappa^{i-1} & \text{if } \xi^i\left(\chi^i,\mathbf{X}\right)=1\\ k_2\kappa^{i-1} & \text{if } \xi^i\left(\chi^i,\mathbf{X}\right)=-1\end{cases}$$

Since $\xi^i\left(\chi^i,\mathbf{X}\right)$ is a spatial function, the information on the oscillations needs to be averaged, so that a scalar value for κ^i can be obtained; this is done as follows:

$$\kappa^i=\min\left\{\left(\frac{\int_\Omega\left(\mu^i\left(\chi^i,\mathbf{X}\right)\right)^{k_3}}{\int_\Omega\psi^i\left(\chi^i,\mathbf{X}\right)}\right)^{-k_3},1\right\},$$

where $k_1\geq 1$, $k_2\leq 1$ and $k_3\leq 1$ are algorithmic parameters. In the numerical examples to be presented, $k_1=1.1$, $k_2=0.5$ and $k_3=0.1$ are used.

5.3. **Algorithm for the topology optimization of incompressible structures subject to FSI.** The sequence of the individual steps is shown in Algorithm 1. Let us explain in detail the proposed strategy.

The main goal of the proposed methodology is to obtain optimized incompressible structures which are subjected to FSI loads. In this sense, we need to specify both a delay for the TO to start, n_{del}, and a time window N_{w}, which will take into account the number of steps to do a TO iteration. Obviously, the selection of this time window is not simple, and it depends upon the FSI problem. For real transient FSI problems, the problem is supposed to be statistically stationary, i.e., some statistics such as the mean or the standard deviation, remain constant [67, 68, 69]. In this work, as a first approximation, a fixed value for the time window is imposed during the whole procedure.

The following ingredient is to compute an additive TD for all the steps along the time window. In each time step, we iterate until convergence of the block-iterative FSI method. Once a converged solution is obtained, we can compute the TD associated with the solid converged state according to Eq. (35) for linear elastic materials or to Eq. (36) for hyperelastic ones. The idea is to sum the contributions for all the time steps inside the time window. To do so, a simple additive function is defined as

$$\mathcal{D}_T^{\text{add}}\mathcal{J}^{n_{\text{w}}+1}\left(\chi,\mathbf{X}\right)=\mathcal{D}_T^{\text{add}}\mathcal{J}^{n_{\text{w}}}\left(\chi,\mathbf{X}\right)+\mathcal{D}_T\mathcal{J}^{n_{\text{w}}}\left(\chi,\mathbf{X}\right),$$

where n_{w} is the time window counter. Once the time window is achieved, $n_{\text{w}}=N_{\text{w}}$, a single TO step is performed for the solid domain with the additive TD according with the flowchart presented in Fig. 1. The counter of steps and the additive TD are reset to zero.

An important aspect to mention is that "dry" TO is performed. This means that only the interior of the structure is optimized, whereas the interface boundary remains constant along the problem. To do so, we split the solid domain Ω_{s}^0 into two sub-domains, Ω_{var} and

Algorithm 1 TO of incompressible structures subject to FSI

Fixed delay steps n_{del} to start the TO procedure and a time window N_{w} to perform a TO step.
$n = 0$; loop over the number of time steps. $n_{\mathrm{w}} = 0$; time window counter to 0.
$n \leftarrow n + 1$
if $n > n_{\mathrm{del}}$ then $n_{\mathrm{w}} \leftarrow n_{\mathrm{w}} + 1$
$k = 0$; iterate coupling iterations until convergence.
$k \leftarrow k + 1$ (block iteration counter omitted in the following).

- **Solve the equations for the solid**, taking into account the tractions coming from the fluid problem $\mathbf{t}_{\mathrm{f}}$.
- **Compute relaxed velocities** on the interface boundary $\mathbf{v}_{\Gamma_{\mathrm{i}}}$ with an Aitken relaxation scheme from the solid velocities $\mathbf{v}_{\Gamma_{\mathrm{i}},\mathrm{s}} = \frac{\delta_2 \mathbf{u}_{\mathrm{s}}}{\delta t}|_{\Gamma_{\mathrm{i}}}$.
- **Compute the domain velocity in the fluid** by solving the mesh equation.
- **Solve the ALE equations for the fluid**, taking into account the mesh velocity $\mathbf{v}_{\mathrm{dom}}$ and using the interface velocity $\mathbf{v}_{\Gamma_{\mathrm{i}}}$.
- **Check convergence and update the unknowns**. Coupling convergence is checked based on the norm of the relative error between coupling iterations of displacements at the interface, i.e., $\|\mathbf{u}_{\Gamma_{\mathrm{i}},\mathrm{s}} - \mathbf{u}_{\Gamma_{\mathrm{i}},\mathrm{f}}\|_{L^2(\Gamma_{\mathrm{i}})}$ and tractions, i.e., $\|\mathbf{t}_{\Gamma_{\mathrm{i}},\mathrm{s}} - \mathbf{t}_{\Gamma_{\mathrm{i}},\mathrm{f}}\|_{L^2(\Gamma_{\mathrm{i}})}$, properly normalized. Convergence is achieved when this norm is below a given tolerance.

End block-iterative loop.

- **Compute the additive TD** associated to the already converged solution at time t^n

$$\mathcal{D}_T^{\mathrm{add}} \mathcal{J}^{n_{\mathrm{w}}+1} = \mathcal{D}_T^{\mathrm{add}} \mathcal{J}^{n_{\mathrm{w}}} + \mathcal{D}_T \mathcal{J}^{n_{\mathrm{w}}},$$

where $\mathcal{D}_T \mathcal{J}^{n_{\mathrm{w}}}$ is the TD associated with time window counter n_{w}..

- Check if $n > n_{\mathrm{del}}$ and $n_{\mathrm{w}} = N_{\mathrm{w}}$, then
  - **Perform a TO step** with the additive TD according to flowchart in Fig. 1.
  $n_{\mathrm{w}} = 0$; restart time window counter.
  $\mathcal{D}_T^{\mathrm{add}} \mathcal{J}^{n_{\mathrm{w}}} = 0$; restart additive topological derivative.
- endif

End loop over the number of time steps.

Ω_{fix}. The former contains the interior of the structure and it is allowed to be optimized during the TO procedure, the latter contains the external layer of the structure in contact with the fluid and is fixed as strong material during the whole TO procedure.

6. Numerical examples

In this section, three numerical examples are presented to assess the performance of the proposed methodology to perform TO of incompressible structures subject to FSI. All numerical examples have been implemented in our in-house code FEMUSS, a multiphysics platform implemented in object oriented Fortran 2008. In the first one, a flow through a channel with a flexible wall is considered to study a stationary solution. The main idea is to analyze the differences between mixed formulations when considering either linear elastic structures or hyperelastic ones. Next, so as to examine the effect of transient FSI solutions, the well-known Turek's test FSI2 is presented. In this case, the behavior of a laminar channel flow around an elastic object is studied when several volume fractions are considered for the optimized structure. To end up, a three-dimensional case with an incompressible flexible plate in a channel flow is considered.

On the one hand, for the fluid sub-problem we select the S-OSGS method with time-dependent SGSs. A maximum of 10 iterations is set, and the numerical tolerance in the $L^2(\Omega_{\mathrm{f}})$ norm is 10^{-5}. On the other hand, for the solid sub-problem the stabilization technique is also selected to be the S-OSGS method. A maximum of 10 iterations is set, and the numerical tolerance in the $L^2\left(\Omega_{\mathrm{s}}^0\right)$ norm is 10^{-5}.

In order to solve the monolithic system of linear equations for each sub-problem, we use the Biconjugate Gradients solver, `BiCGstab` [70], which is already implemented in the `PETSc` parallel solver library [71].

Concerning the iterative scheme, a strong-coupling staggered approach is considered, as previously mentioned. For the transmission conditions on the interface boundary Γ_{i}, the relative tolerance is set to 10^{-3}. For the mapping between domains, the aforementioned ALE formulation is applied in the fluid domain, together with the Total Lagrangian approach for the solid mechanics problem

With regards to the TO parameters, the weak material is considered to be compressible, with $\nu_{\mathrm{wea}} = 0.4$. The mixed formulation for the solid is used in this region even if it is not strictly required to avoid switching formulations and changing the number of total unknowns during the simulation. The jump of stiffness γ is fixed to 10^{-2}. As a stopping criterion for the TO algorithm, we impose a relative tolerance for the objective functional $\mathrm{tol} = 10^{-3}$, unless otherwise specified. The volume fraction is reduced at once except where otherwise stated. In all presented figures, only the positive part of the level set is plotted, therefore only the strong material part is shown. The rest is filled of weak material elements, and thus interpreted as the void region.

6.1. **Beam in a channel flow.** In this first problem, we seek to determine the optimal topology of a structure immersed in a channel flow. This example is very similar to the one presented in [37, 43]. The problem presented here has a fixed interface boundary between the fluid flow and the structure. Therefore, we optimize the interior of the solid. The geometry of the problem is shown in Fig. 2

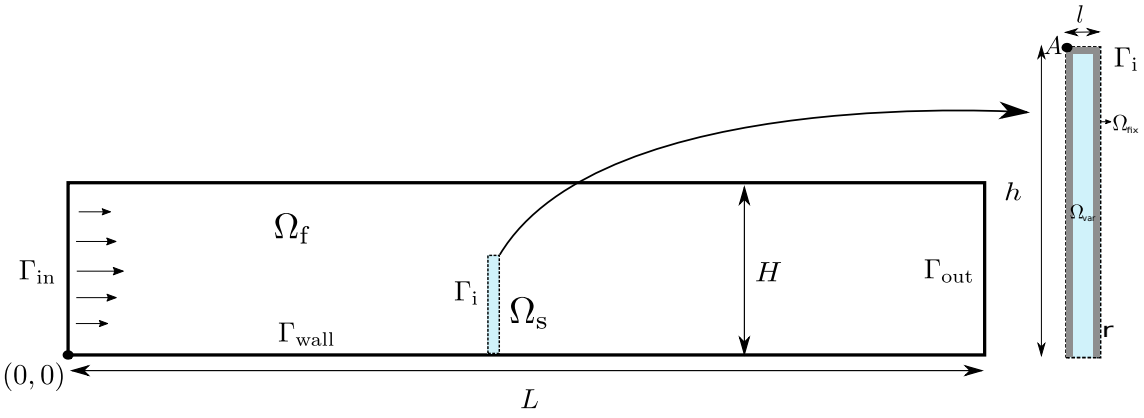

FIGURE 2. Beam in a channel flow. Geometry.

Regarding the channel measures, the rigid channel has height $H = 1$ m. The flexible wall is located at $2H$ from the channel entrance. The length of the whole channel is $L = 5$ m. The structure bar has length $l = 0.1$ m and height $h = 0.5$ m. The solid domain Ω_{s}^0 is divided into two subdomains Ω_{var} and Ω_{fix}. The former contains the interior of the structure and it is allowed to be optimized during the TO procedure, the latter contains the external layer of the structure of width $r = 0.01$ m which is in contact with the fluid and is fixed as strong material during the whole TO procedure.

Regarding the properties of the fluid, the density is $\rho_{\mathrm{f}} = 1$ kg/m^3 and the dynamic viscosity is $\mu_{\mathrm{f}} = 1$ Pa $\cdot$ s. For the elastic plate the properties are as follows: an initial density $\rho_{\mathrm{s}}^0 = 1$ kg/m^3, a Young's modulus $E_{\mathrm{s}} = 40$ kPa and a Poisson's ratio $\nu_{\mathrm{s}} = 0.5$. A plane strain assumption is considered. A final volume of 50% of the initial one is stated as a volume restriction for Ω_{var}.

Concerning the boundary conditions, in the inlet boundary of the fluid domain Γ_{in}, a steady Poiseuille flow with average velocity $\bar{v}_{\text{in}}$ is assumed, given by

$$\bar{v}_{\text{f}}(0, y) = 1.5\, \bar{v}_{\text{in}} \frac{y(H-y)}{\left(\frac{H}{2}\right)^2}.$$

On the walls Γ_{wall}, no-slip boundary conditions are imposed, and in the outlet Γ_{out}, the pressure is set to $p_{\text{out}} = 0$ Pa. A rectangular plate is considered as the solid domain, and it is clamped at the bottom side.

The domains are discretized using P_1 (linear) elements for both fluid and solid domains. Regarding the distribution of the elements, both meshes are unstructured. In total, the fluid mesh is formed by 12 446 elements, and the solid mesh by 12 720 elements as it is shown in Fig 3.

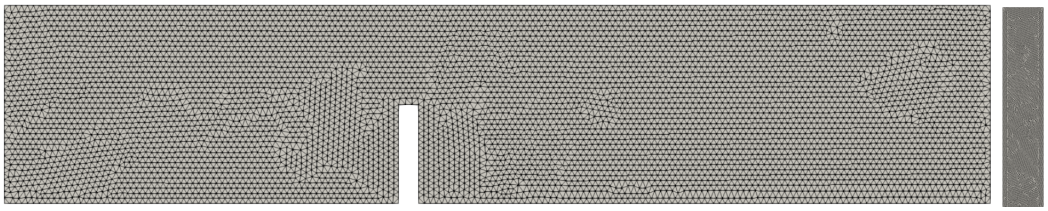

(A) Fluid mesh (B) Solid mesh

FIGURE 3. Beam in a channel flow. Mesh domains.

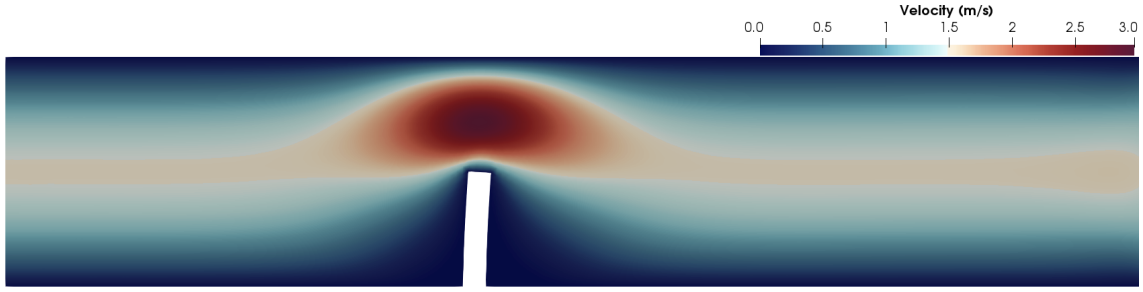

(A) Velocity field

(B) Pressure field

FIGURE 4. Beam in a channel flow. Distribution of the velocity field (top) and pressure (bottom) in the fluid domain with average velocity $\bar{v}_{\text{in}} = 1$ m/s. Velocities are plotted using their Euclidean norm.

To start the problem, a smooth increase of the velocity profile in time is prescribed, given by

$$v_{\mathrm{f}}(0,y,t) = \begin{cases} \bar{v}_{\mathrm{f}}(0,y)\frac{1-\cos\frac{\pi}{2}t}{2} & \text{if } t < 1.0 \text{ s} \\ v_{\mathrm{f}}(0,y) & \text{otherwise} \end{cases}.$$

We select the time step $\delta t = 0.005$ s. During the first 2.5 s, we let the FSI problem run without performing any TO iteration. To do so, we impose a delay in the TO procedure of $n_{\mathrm{del}} = 500$. At this moment, the problem has already converged to a stationary solution. From this point on, we select a time window of $N_{\mathrm{w}} = 50$, so that $N_{\mathrm{w}}\delta t = 0.25$ s, to store the additive TD and perform a TO iteration. We continue the same procedure until a converged optimized solution is obtained for the structure.

First of all, let us consider the case $\bar{v}_{\mathrm{in}} = 1$ m/s, which results in a fluid flow with Reynolds number $\mathrm{Re} = 1$. For this case, the final stationary FSI solution is supposed to produce very small strains in the structure, which can be approximated with the infinitesimal strain theory. Let us start by showing the final stationary solution for the fluid domain once the optimized structure has been obtained for a linear elastic material. Both velocity and pressure fields in the channel are depicted in Fig. 4.

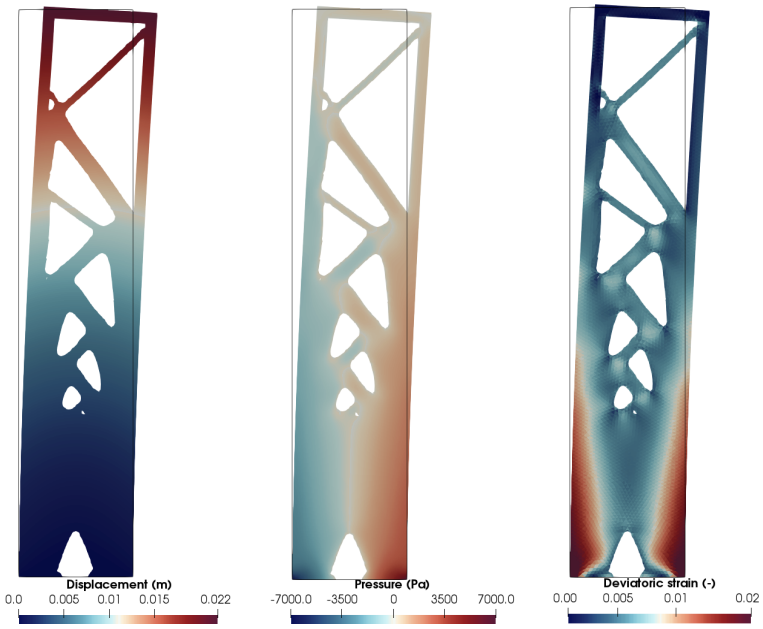

(A) Displacement field

(B) Pressure field

(C) Deviatoric strain field

FIGURE 5. Beam in a channel flow. Distribution of the displacement field (left), pressure (middle) and deviatoric strain field (right) in the linear elastic incompressible beam with **u**-p formulation and with average velocity $\bar{v}_{\mathrm{in}} = 1$ m/s. Displacements and deviatoric strains are plotted using their Euclidean norm.

We consider the two different formulations presented in Subsection 3.1 for the structure. In Fig. 5 the final optimized solution with the **u**-p formulation is shown, whereas in Fig. 6 the one obtained for the three-field **u**-p-**e** formulation is presented. Both solutions

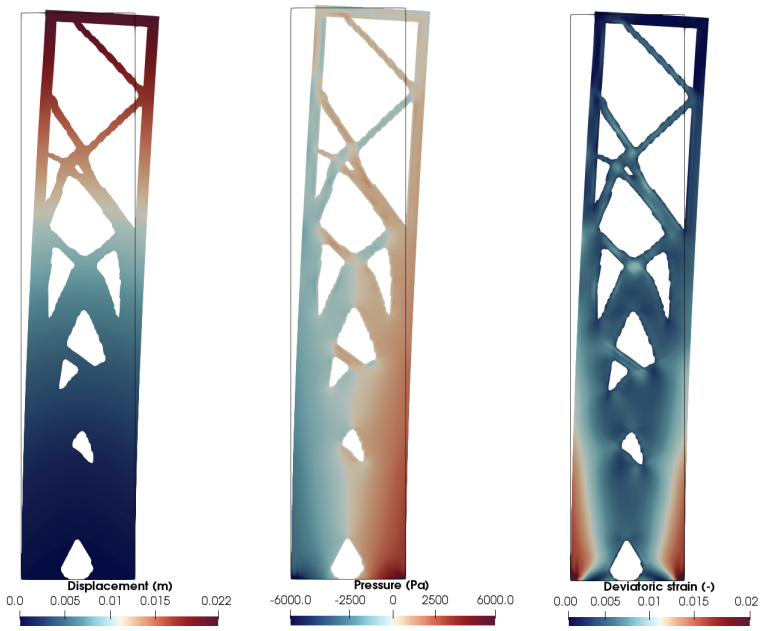

(A) Displacement field

(B) Pressure field

(C) Deviatoric strain field

FIGURE 6. Beam in a channel flow. Distribution of the displacement field (left), pressure (middle) and deviatoric strain field (right) in the linear elastic incompressible beam with **u**-p-**e** formulation and with average velocity $\bar{v}_{\text{in}} = 1$ m/s. Displacements and deviatoric strains are plotted using their Euclidean norm.

display different features, although they are supposed to converge to the same one with finer meshes. We refer the readers to [21] for an in-depth comparison of the accuracy and performance of both formulations.

Let us consider now a hyperelastic material. The solution of the channel flow is very similar as the one obtained for the linear elastic case. Again, the two different formulations presented in Subsection 3.2 are applied. Fig. 7 presents the final solution obtained with the two-field **u**-p formulation and Fig. 8 displays the solution for the **u**-p-$\mathbf{S}'$ formulation. Again quite different solutions are obtained due to the nonlinearities of the problem, the iterative TO algorithm and the coarse mesh of the solid domain that we are considering.

For the sake of completeness, Table 1 shows the forces exerted by the fluid flow on the whole submerged beam structure and the displacement at point A for the different cases we have studied. As it was expected, all cases display the same final properties due to the fact that infinitesimal strain theory can be considered.

Finally, in Fig. 9 the total potential energy is plotted against the TO iterations during the whole procedure for all the formulations considered. As expected, all formulations are decreasing the objective functional during the TO iterations until a minimum is achieved. Due to the high accuracy of strains and stresses that are obtained using the three-field formulations, we can see different values for the total potential energy. Obviously, this difference is expected to be reduced while refining the solid mesh.

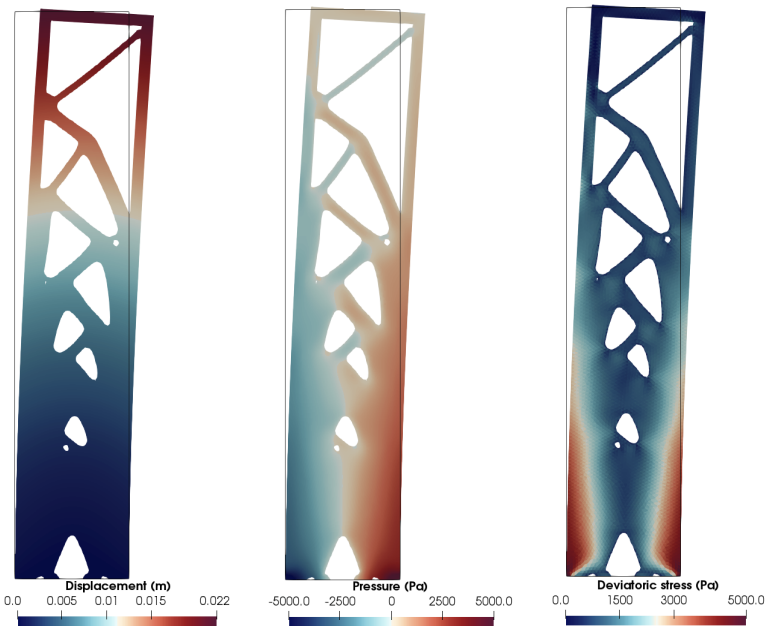

(A) Displacement field

(B) Pressure field

(C) Deviatoric PK2 stress field

FIGURE 7. Beam in a channel flow. Distribution of the displacement field (left), pressure (middle) and deviatoric PK2 stress field (right) in the hyperelastic incompressible beam with **u**-p formulation and with average velocity $\bar{v}_{\text{in}} = 1$ m/s. Displacements and deviatoric stresses are plotted using their Euclidean norm.

	u_x [10^{-1} m]	u_y[10^{-2} m]	**drag** [N]	**lift** [N]
without TO	0.1978	0.2208	86.3563	-11.9159
u-p, LE	0.2168	0.2791	86.5657	-12.1485
u-p-**e**, LE	0.2144	0.2791	86.6162	-12.1428
u-p, HE	0.2218	0.2346	86.2957	-12.1737
u-p-$\mathbf{S}'$, HE	0.2230	0.2304	86.2634	-12.1846

TABLE 1. Beam in a channel flow. Displacement at point A and forces exerted by the fluid on the whole submerged body with average velocity $\bar{v}_{\text{in}} = 1$ m/s. LE states for a linear elastic material and HE for a hyperelastic one.

Let us now consider a case which involves finite strains. To do so, we increment the average velocity to $\bar{v}_{\text{in}} = 10$ m/s, which results in a fluid flow with Reynolds number $\text{Re} = 10$. To perform this study we employ only the **u**-p formulation for both linear elastic and hyperelastic materials. Fig. 10 shows the solution for the fluid domain which is quite similar in both cases. Figs. 11-12 show the final optimized structure for a linear elastic material and for a hyperelastic one, respectively. In this case, we can observe that strains are not infinitesimal anymore.

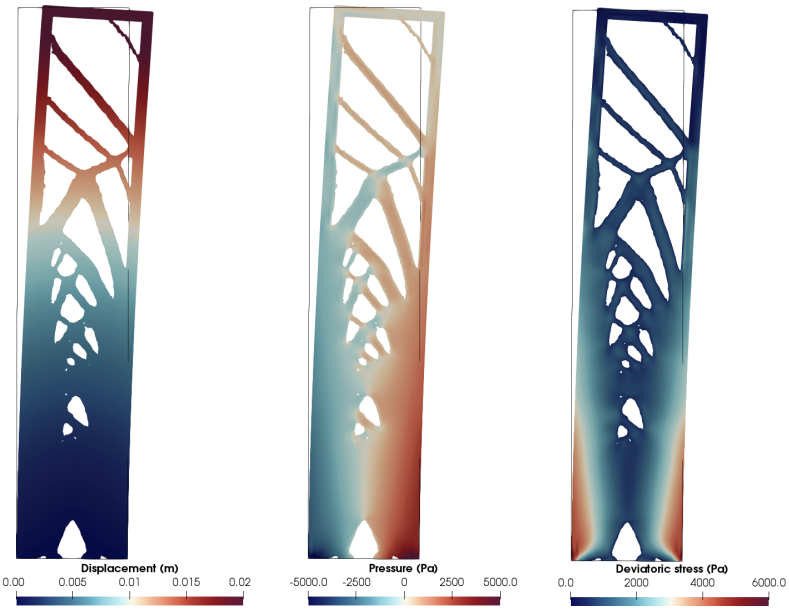

(A) Displacement field

(B) Pressure field

(C) Deviatoric PK2 stress field

FIGURE 8. Beam in a channel flow. Distribution of the displacement field (left), pressure (middle) and deviatoric PK2 stress field (right) in the hyperelastic incompressible beam with **u**-p-$\mathbf{S}'$ formulation and with average velocity $\bar{v}_{\text{in}} = 1$ m/s. Displacements and deviatoric stresses are plotted using their Euclidean norm.

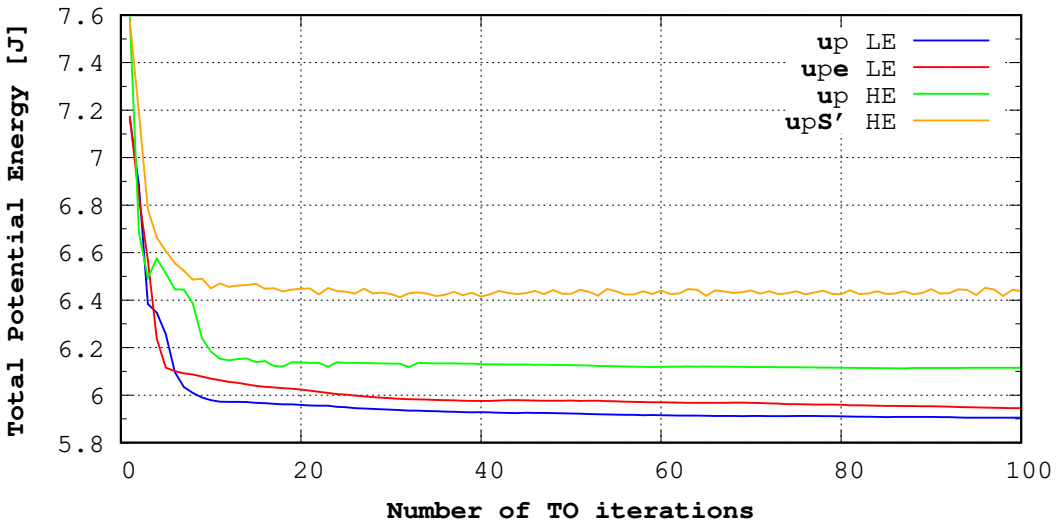

FIGURE 9. Beam in a channel flow. Convergence diagrams for all formulations with average velocity $\bar{v}_{\text{in}} = 1$ m/s. LE states for a linear elastic material and HE for a hyperelastic one.

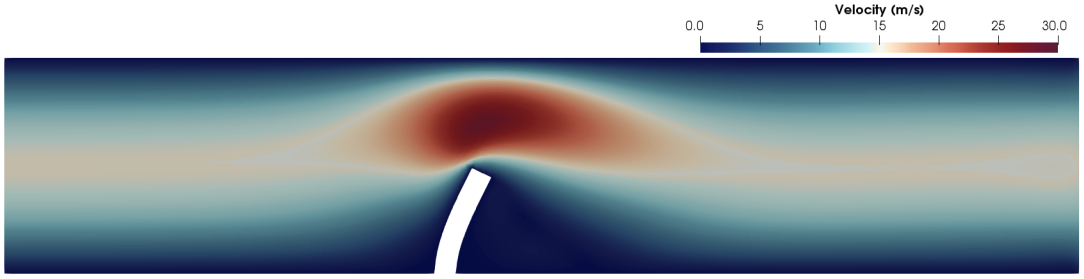

(A) Velocity field

(B) Pressure field

FIGURE 10. Beam in a channel flow. Distribution of the velocity field (top) and pressure (bottom) in the fluid domain with average velocity $\bar{v}_{\text{in}} = 10$ m/s. Velocities are plotted using their Euclidean norm.

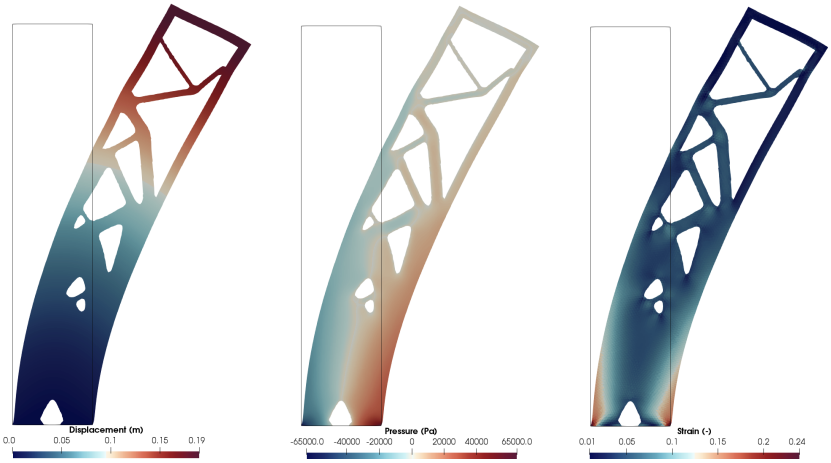

(A) Displacement field

(B) Pressure field

(C) Infinitesimal strain field

FIGURE 11. Beam in a channel flow. Distribution of the displacement field (left), pressure (middle) and infinitesimal strain tensor field (right) in the linear elastic incompressible beam with $\mathbf{u}$-p formulation and with average velocity $\bar{v}_{\text{in}} = 10$ m/s. Displacements and strains are plotted using their Euclidean norm.

To show that the linear elastic theory hypothesis is not suitable in this case, Table 2 shows the fluid forces on the beam interface and the displacement at point A. As it can

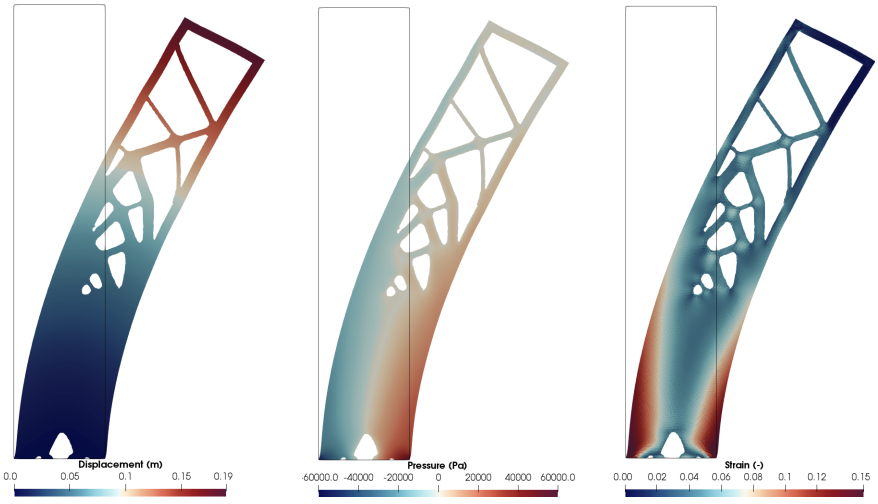

(A) Displacement field

(B) Pressure field

(C) Green Lagrange strain tensor field

FIGURE 12. Beam in a channel flow. Distribution of the displacement field (left), pressure (middle) and Green Lagrange strain tensor field (right) in the hyperelastic incompressible beam with **u**-p formulation and with average velocity $\bar{v}_{\text{in}} = 10$ m/s. Displacements and strains are plotted using their Euclidean norm.

be clearly seen, quite different solutions are obtained between the linear elastic model and the finite strain hyperelastic one. This example clearly shows that even in stationary FSI problems, the linear theory of elasticity must be considered only when very small strains (smaller than 10^{-3}, typically) are produced in the structure. From the conceptual point of view, in this case there is no physical interaction, as the solid configuration does not change and thus the solid does not affect the fluid dynamics.

	u_x [m]	$u_y[10^{-1}$ m]	**drag** [N]	**lift** [N]
without TO, LE	0.1797	0.2351	1071.6400	-192.8160
u-p, LE	0.1969	0.2531	1081.8600	-214.3030
without TO, HE	0.1758	-0.0972	887.3970	-166.3880
u-p, HE	0.1878	-0.1360	867.1500	-171.931

TABLE 2. Beam in a channel flow. Displacement at point A and forces exerted by the fluid on the whole submerged body with average velocity $\bar{v}_{\text{in}} = 10$ m/s. LE states for a linear elastic material and HE for a hyperelastic one.

6.2. **Turek's test.** In this second case, we study the TO of an incompressible hyperelastic structure subject to FSI with a laminar flow. This case derives from the well-known benchmark in FSI used by many authors [72]. The configuration consists of a laminar channel flow around an elastic object which results in self-induced oscillations of the structure.

The geometry of the problem is displayed in Fig. 13. The rigid channel has height $H = 0.41$ m and length $L = 2.5$ m. The circle centre is positioned at point $C = (0.2, 0.2)$ m (measured from the left bottom corner of the channel) and its radius is $r = 0.05$ m.

The solid bar has a length $l = 0.35$ m and a height $h = 0.02$ m. The right bottom corner is positioned at $(0.6, 0.19)$ m, and the left end is fully attached to the fixed cylinder. The solid domain Ω_{s}^0 is divided into two subdomains Ω_{var} and Ω_{fix}. The former contains the interior of the structure and it is allowed to be optimized during the TO procedure, the latter contains the external layer of the structure of width $d = 0.001$ m, which is in contact with the fluid and is fixed as strong material during the whole TO procedure.

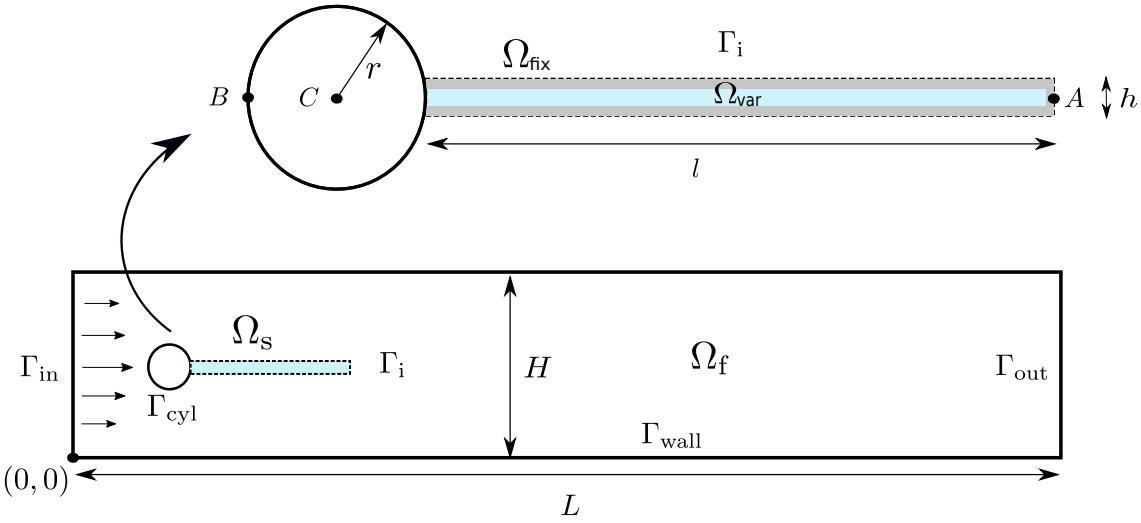

FIGURE 13. Turek's test. Geometry.

With regards to boundary conditions, a parabolic profile is prescribed at the left channel inflow, given by

$$\bar{v}_{\mathrm{f}}(0, y) = 1.5\, \bar{v}_{\mathrm{in}} \frac{y(H - y)}{\left(\frac{H}{2}\right)^2},$$

such that the mean inflow velocity is $\bar{v}_{\mathrm{in}}$ and the maximum of the inflow velocity profile is $1.5\bar{v}_{\mathrm{in}}$. A smooth increase of the velocity profile in time is prescribed, given by

$$v_{\mathrm{f}}(0, y, t) = \begin{cases} \bar{v}_{\mathrm{f}}(0, y) \frac{1 - \cos \frac{\pi}{2} t}{2} & \text{if } t < 2.0 \text{ s} \\ \bar{v}_{\mathrm{f}}(0, y) & \text{otherwise} \end{cases}.$$

The outflow condition is considered stress free. Finally, a no-slip condition is prescribed for the fluid on the other boundary parts. Concerning the boundary conditions of the structure, fixed null displacement is considered at the left edge.

The main goal of this example is to perform a TO procedure of a transient FSI solution. Therefore, the FSI2 parameter settings are taken from the benchmark. The mean flow velocity is fixed to $\bar{v}_{\mathrm{in}} = 1$ m/s. Regarding the properties of the fluid, the density is $\rho_{\mathrm{f}} = 1\,000$ kg/m^3 and the dynamic viscosity is $\mu_{\mathrm{f}} = 1$ Pa $\cdot$ s. This results in a flow with Reynolds number $\mathrm{Re} = 100$. For the incompressible elastic plate the properties are as follows: an initial density $\rho_{\mathrm{s}}^0 = 10\,000$ kg/m^3, a Young's modulus $E_{\mathrm{s}} = 14$ kPa and a Poisson's ratio $\nu_{\mathrm{s}} = 0.5$. The plane strain assumption is considered.

The domains are discretized using P_1 (linear) elements for both sub-domains. Regarding the distribution of the elements in the fluid domain, the mesh is finer around the cylinder and the bar, while downstream the mesh is coarser. In total, the fluid mesh is formed by 13 537 unstructured elements, and the solid mesh by 15 608 unstructured elements equally distributed over the bar as it can be observed in Fig. 14

We select the time step $\delta t = 0.005$ s. During the first 12 s, we let the FSI problem run without performing any TO iteration. This is the time needed to arrive to a periodic solution. To do so, we impose a delay in the TO procedure of $n_{\mathrm{del}} = 2\,400$. From this

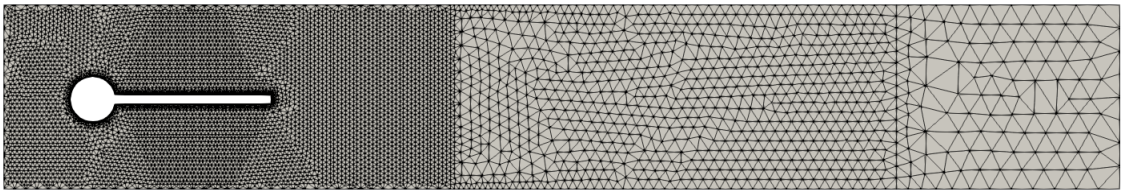

(A) Fluid mesh domain

(B) Solid mesh domain

FIGURE 14. Turek's test. Mesh domains.

point on, we select a time window of $N_{\mathrm{w}} = 50$, so that $N_{\mathrm{w}}\delta t = 0.25$ s, to store the additive TD and perform a TO iteration. This time is very close to the period in the case without TO. We continue the same procedure until a converged optimized solution is obtained for the structure. For this example, only the **u**-p formulation is considered.

To show the effect of the TO procedure in a transient FSI problem, we select several volume fractions, ranging from 90% to 70%. Let us first impose a final volume of 90% of the initial one. Fig. 15 shows both the velocity and the pressure fields at different times of the final transient solution. The final optimized structure is depicted in Fig. 16. As expected, all the extracted material is taken from the right edge of the beam. Next, we select a final volume of 80% of the initial one. Figs. 17-18 display both the final solutions for the fluid domain and the optimized solid structure at different times, respectively. In this case, oscillations decrease compared to the ones presented in the first case. This reduction is clearly explained due to the loss of mass in the structure. Finally, we impose a final volume of 70% of the initial one. In this case, an almost stationary solution is achieved as it can be seen in Figs. 19-20. From this study, we can draw the conclusion that TO optimization cannot only be used for reducing material volumes while minimizing an objective function, but to modify transient solutions in time by changing oscillations in some coupled problems.

To show clearly the effects that are exposed in the previous paragraph, both forces exerted by the fluid in the whole submerged body (cylinder plus beam) and displacement at point A are plotted in Fig. 21 for all volume fractions considered. All volume fractions arrive with the same oscillations at time $t = 12$ s. At this point each one decreases to the final volume fraction required. As it can be seen, drag and lift are decreasing while decreasing the final volume fraction and therefore, the displacement at point A is also decreasing. For the case of 70% of the final volume, we can see that all figures end with a stationary solution.

To end this example, in Fig. 22 the evolution of the total potential energy for the three cases along TO iterations is shown. As it is expected, the functional decreases for the three cases until a point in which we consider that a minimum is achieved. It is worth to mention that in the 70% case, the stationary solution means that almost no forces are done by the fluid flow to the solid, and this is the reason why the energy is almost 0. Let us also point out that some oscillations appear in the 90% case due to the fact that the compliance in this case depends also upon time. If we want to remove this effect, a higher time window for the TO iterations should be considered.

6.3. **Flexible plate in a channel flow.** As a final example we study the optimization of the internal structural layout of a three-dimensional test case which exhibits high non-linearities and a final stationary FSI solution. The problem geometry is depicted in Fig.

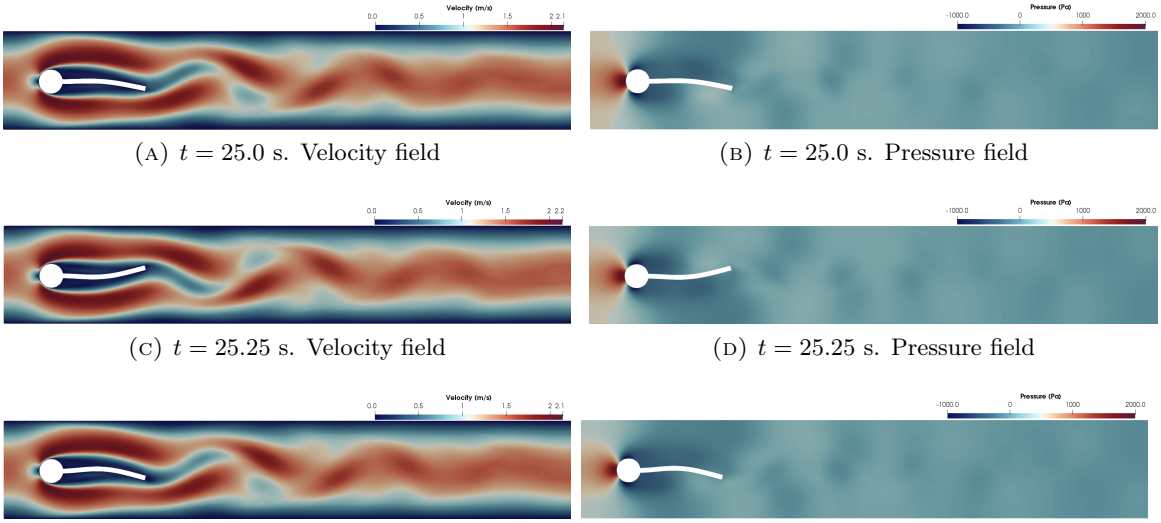

(A) $t = 25.0$ s. Velocity field

(B) $t = 25.0$ s. Pressure field

(C) $t = 25.25$ s. Velocity field

(D) $t = 25.25$ s. Pressure field

(E) $t = 25.5$ s. Velocity field

(F) $t = 25.5$ s. Pressure field

FIGURE 15. Turek's test. Distribution of the velocity field (left) and pressure (right) in the fluid domain with 90% of final volume at several times. Velocities are plotted using their Euclidean norm.

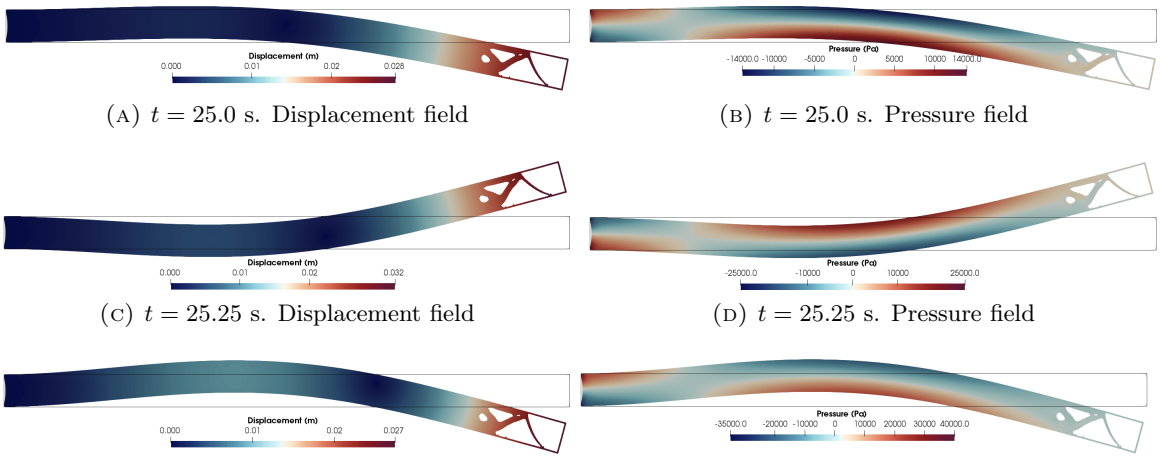

(A) $t = 25.0$ s. Displacement field

(B) $t = 25.0$ s. Pressure field

(C) $t = 25.25$ s. Displacement field

(D) $t = 25.25$ s. Pressure field

(E) $t = 25.5$ s. Displacement field

(F) $t = 25.5$ s. Pressure field

FIGURE 16. Turek's test. Distribution of the displacement field (left) and pressure (right) in the solid domain with 90% of final volume at several times. Displacements are plotted using their Euclidean norm.

23. A plate of length $l = 0.07$ m, width $w = 0.6$ m and height $h = 0.35$ m is mounted at the bottom of a channel. The plate is located at $L_1 = 0.49$ m from the channel entrance. The channel is a cuboid-shaped domain of length $L = 1.5$ m, width $W = 1.2$ m and height $H = 0.6$ m. The solid domain Ω_{s}^0 is divided into two subdomains Ω_{var} and Ω_{fix}. The former contains the interior of the structure and it is allowed to be optimized during the TO procedure, the latter contains the external layer of the structure of width $r = 0.007$ m which is in contact with the fluid and is fixed as strong material the whole TO procedure.

A parabolic profile for the velocity at the channel inlet face is prescribed, given by

$$\bar{v}_{\mathrm{f}}(0, y, z) = \bar{v}_{\max} \frac{2500}{81} z\,(z - 0.6)\,(y + 0.6)\,(y - 0.6)\,,$$

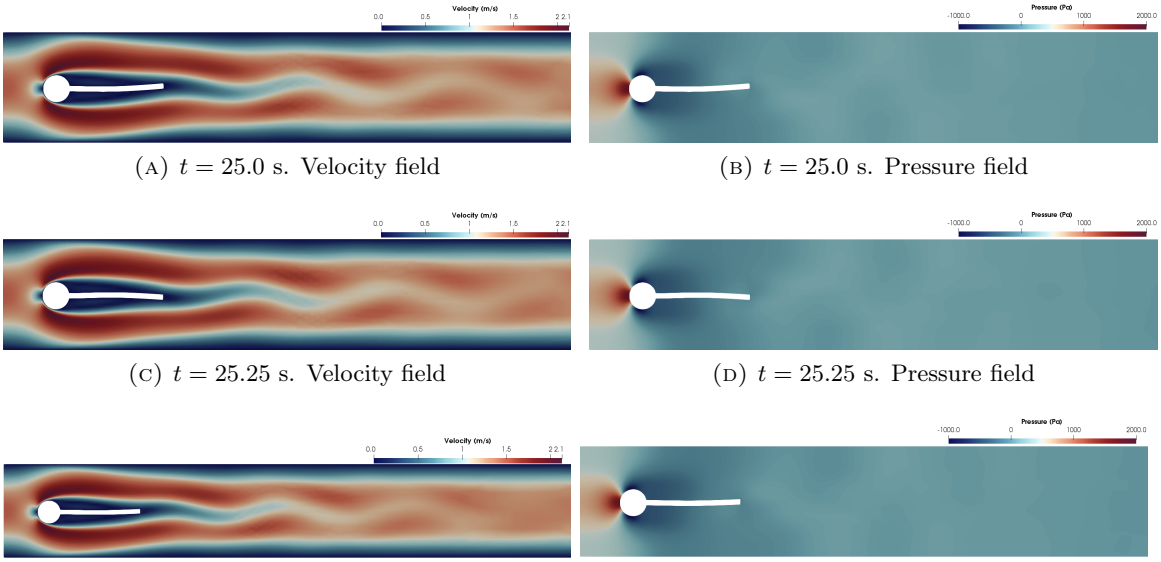

(A) $t = 25.0$ s. Velocity field

(B) $t = 25.0$ s. Pressure field

(C) $t = 25.25$ s. Velocity field

(D) $t = 25.25$ s. Pressure field

(E) $t = 25.5$ s. Velocity field

(F) $t = 25.5$ s. Pressure field

FIGURE 17. Turek's test. Distribution of the velocity field (left) and pressure (right) in the fluid domain with 80% of final volume at several times. Velocities are plotted using their Euclidean norm.

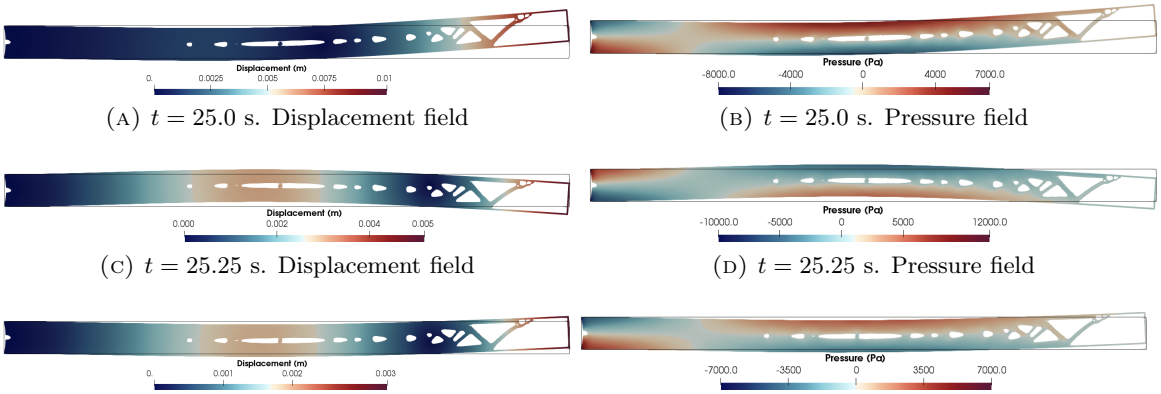

(A) $t = 25.0$ s. Displacement field

(B) $t = 25.0$ s. Pressure field

(C) $t = 25.25$ s. Displacement field

(D) $t = 25.25$ s. Pressure field

(E) $t = 25.5$ s. Displacement field

(F) $t = 25.5$ s. Pressure field

FIGURE 18. Turek's test. Distribution of the displacement field (left) and pressure (right) in the solid domain with 80% of final volume at several times. Displacements are plotted using their Euclidean norm.

where the maximum velocity is $\bar{v}_{\max} = 1$ m/s and it is varied by a temporal factor

$$v_{\mathrm{f}}(0, y, z, t) = \begin{cases} \bar{v}_{\mathrm{f}}(0, y, z) \frac{1 - \cos \frac{\pi}{2} t}{2} & \text{if } t < 0.1 \text{ s} \\ \bar{v}_{\mathrm{f}}(0, y, z) & \text{otherwise} \end{cases}.$$

The time $t = 0.1$ s denotes the final time of the excitation phase. Therefore, the flow entering the domain excites the structural flap to initially bend and deform. No-slip wall boundary conditions at the four sides perpendicular to the inlet prevent the flow to escape. A stress-free condition is applied on the outlet boundary. The bottom face of the flexible plate is considered clamped.

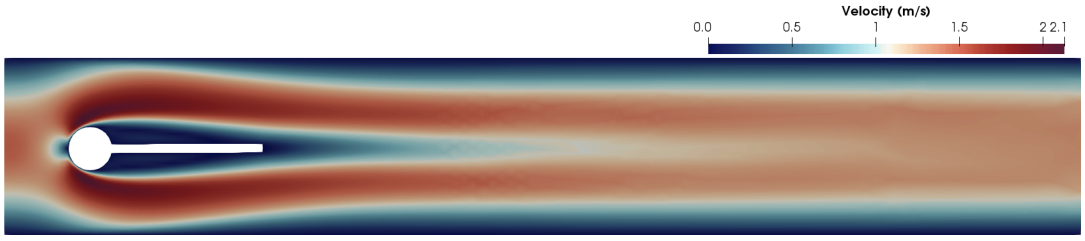

(A) Velocity field

(B) Pressure field

FIGURE 19. Turek's test. Distribution of the velocity field (top) and pressure (bottom) in the fluid domain with 70% of final volume. Velocities are plotted using their Euclidean norm.

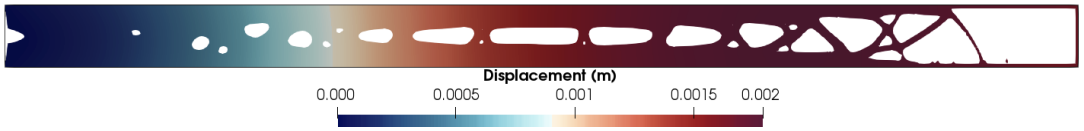

(A) Displacement field

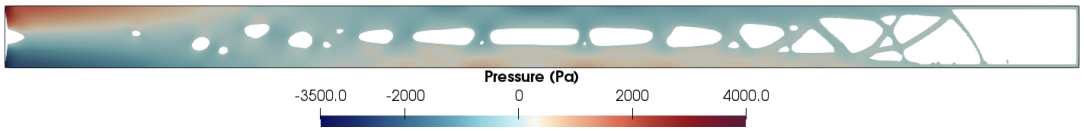

(B) Pressure field

FIGURE 20. Turek's test. Distribution of the displacement field (top) and pressure (bottom) in the solid domain with 70% of final volume. Displacements are plotted using their Euclidean norm.

The material properties are chosen as follows: the flow is assumed incompressible with dynamic viscosity $\mu_f = 0.01$ Pa $\cdot$ s and a density $\rho_f = 1$ kg/m^3. Based on the maximum inflow velocity and the width of the flap, the Reynolds number Re ranges from 0–60. The structure is assigned a Young's modulus $E_s = 3\,000$ Pa, a Poisson's ratio $\nu_s = 0.5$ and an initial density $\rho_s^0 = 250$ kg/m^3, for which finite and dynamic deformations are expected. A final volume of 60% of the initial one is fixed as a volume restriction for Ω_{var}.

The domains are discretized using tetrahedral elements for both fluid and solid domains. Regarding the distribution of the elements, both meshes are unstructured and with smaller elements concentrated on the interface boundary. In total, the fluid mesh is formed by 140 600 elements, and the solid mesh by 660 000 elements.

We select the time step $\delta t = 0.001$ s. During the first 0.6 s, we let the FSI problem run without performing any TO iteration. To do so, we impose a delay in the TO procedure of $n_{del} = 600$. At this moment, the problem converges to a stationary solution. From

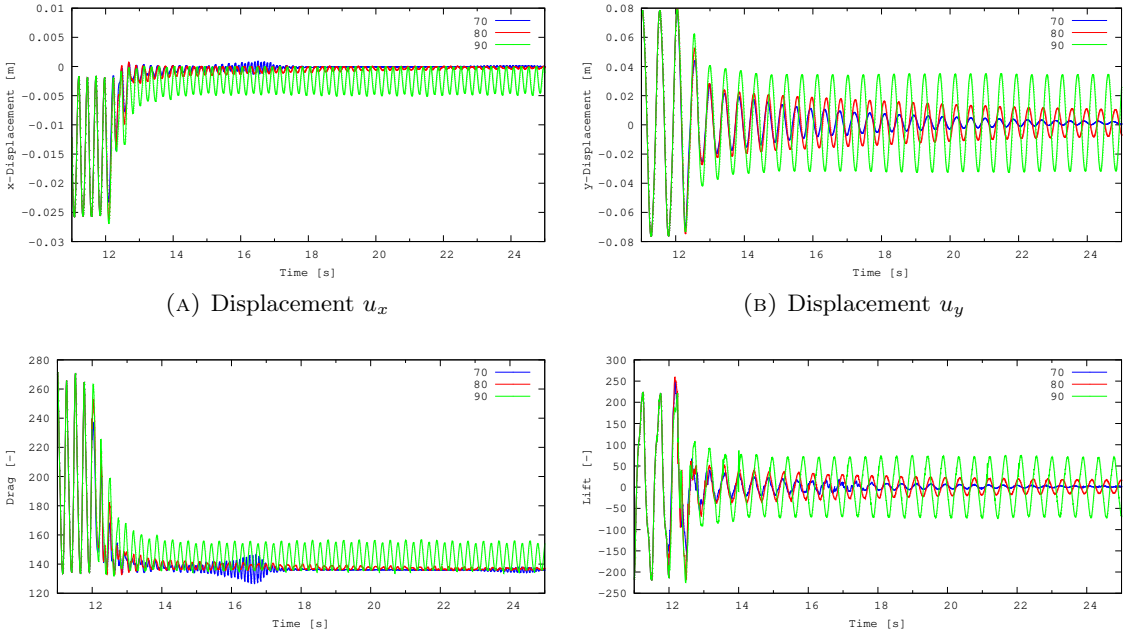

(A) Displacement u_x

(B) Displacement u_y

(C) Drag

(D) Lift

FIGURE 21. Turek's test. Displacement at point A and forces exerted by the fluid on the whole submerged body.

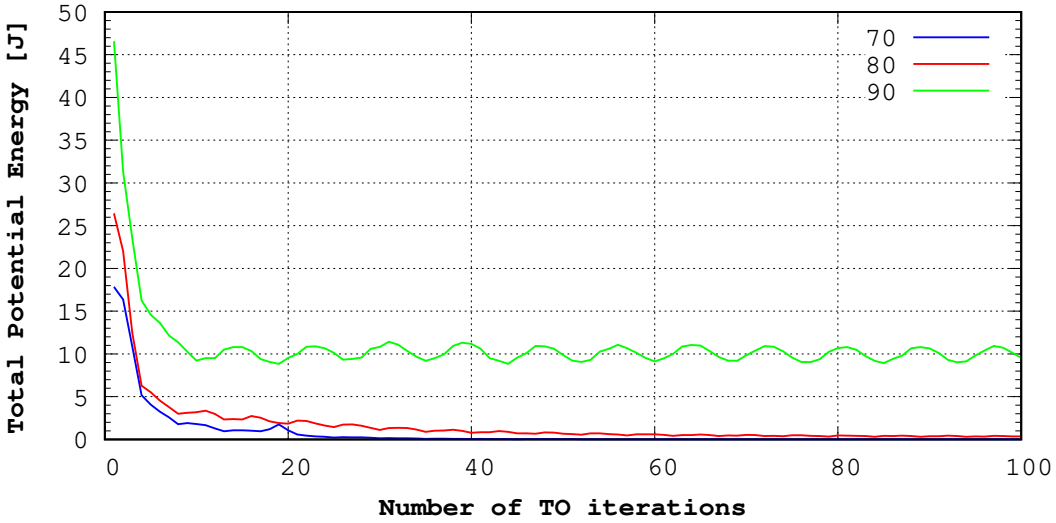

FIGURE 22. Turek's test. Convergence diagram for all the volume fractions studied.

this point on, we select a time window of $N_{\mathrm{w}} = 50$, so that $N_{\mathrm{w}}\delta t = 0.05$ s, to store the additive TD and perform a TO iteration. We continue the same procedure until a converged optimized solution is obtained for the structure. For this example, only the **u**-p formulation is considered.

First of all, let us show the final stationary FSI solution in Fig. 24. As explained before, "dry" TO is performed and therefore the boundary of the solid which is in contact with the fluid flow remains constant. It is important to mention that strains of the order of 10^{-1} are obtained, which means that the infinitesimal strain theory is not suitable in this case

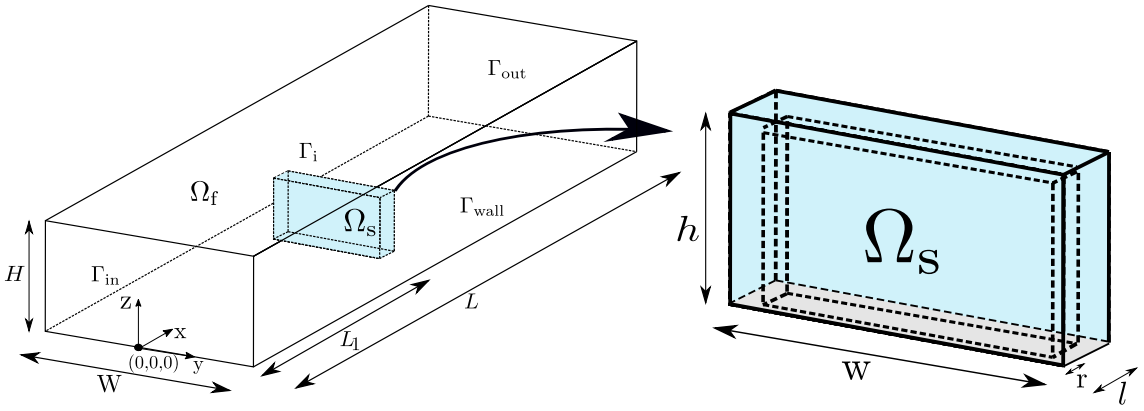

FIGURE 23. Flexible plate in a channel flow. Geometry.

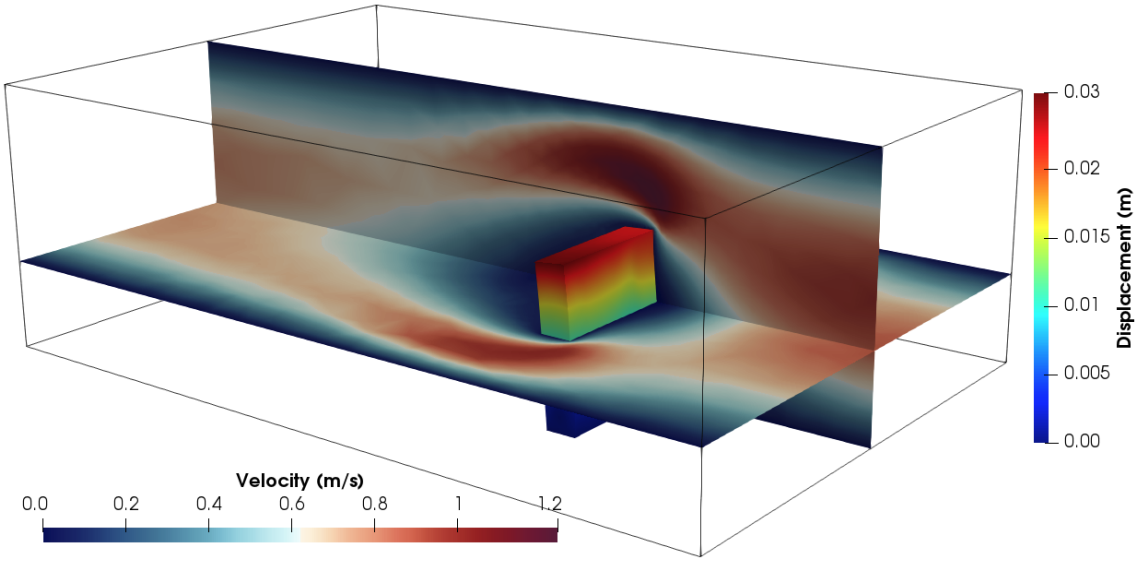

FIGURE 24. Flexible plate in a channel flow. Final stationary solution.

and finite strain theory fits better with the kind of problem that we are modeling. Both velocity and pressure fields in the channel flow from different points of view are depicted in Fig. 25.

Let us move now to the solid domain. Fig. 26 displays the final optimized incompressible structure once a stationary solution is achieved and the objective function is not decreasing anymore (according to the tolerance). To show the interior of the solid, which is the one which is optimized, a cut of the middle of the structure is depicted from different viewpoints and the fixed part and the empty region are shown in grey. For the sake of completeness, in Fig. 27 the evolution of both the total potential energy and the volume fraction during the TO iterations is shown. As expected, the objective function increases while we start decreasing the volume fraction progressively, just to avoid numerical problems due to the highly nonlinear behavior of the whole problem. Once the volume fraction of 60 % is fixed, the objective function starts decreasing until a minimum is obtained and, therefore, the problem is ended.

7. CONCLUSIONS

In this work, a TO algorithm has been presented to deal with incompressible structures subjected to FSI loads. The main goal of this work was to combine an additive TD with a

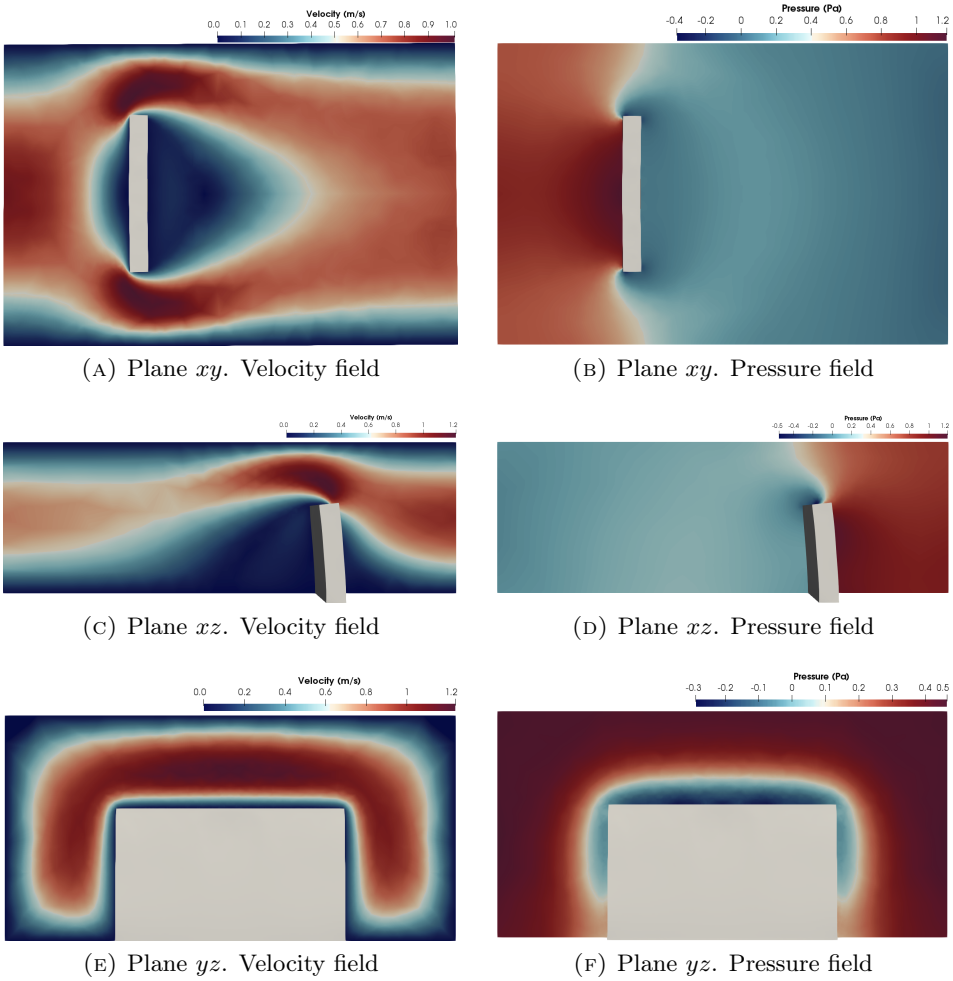

(A) Plane xy. Velocity field

(B) Plane xy. Pressure field

(C) Plane xz. Velocity field

(D) Plane xz. Pressure field

(E) Plane yz. Velocity field

(F) Plane yz. Pressure field

FIGURE 25. Flexible plate in a channel flow. Distribution of the velocity field (left) and pressure (right) in the fluid domain. Velocities are plotted using their Euclidean norm.

level set method to optimize the internal structural layout of FSI problems. The structural response is modeled assuming either infinitesimal strains or finite ones. The fluid model is studied with the incompressible Navier-Stokes model and the coupling problem is treated in a staggered way with strong-coupling between sub-problems.

The key to solving problems involving incompressible structures was the introduction of the mixed stabilized FE formulations presented in Subsection 3.1 for linear elastic materials and in Subsection 3.2 for hyperelastic ones. On the one hand, the well-known $\mathbf{u}$-p formulation, in which the pressure is added as an unknown—the fundamental one, when dealing with incompressible materials. On the other hand, three-field formulations which also add stresses as unknowns of the problem to increase their accuracy.

Thanks to the TD formulae that are presented in [29], the TO algorithm of incompressible structures is possible for linear elastic materials by means of the topological derivative concept. Furthermore, the approximation applied to the TD in the finite strain cases, replacing it by the minimization direction given in Eq. (36), shows good performance in the numerical examples presented in this work, in the sense that the objective functional certainly decreases along the TO steps.

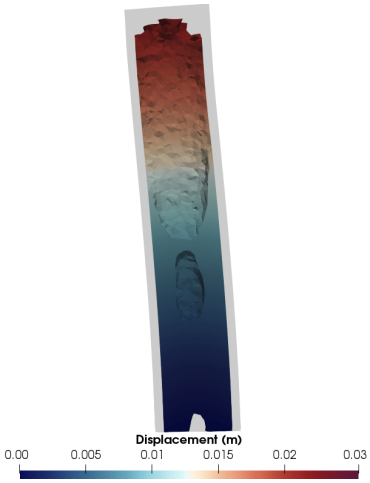

(A) Plane xz. Displacement field

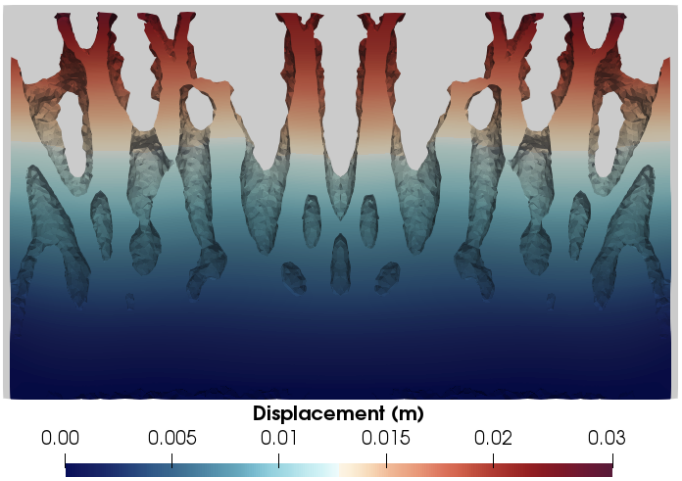

(B) Plane yz. Displacement field

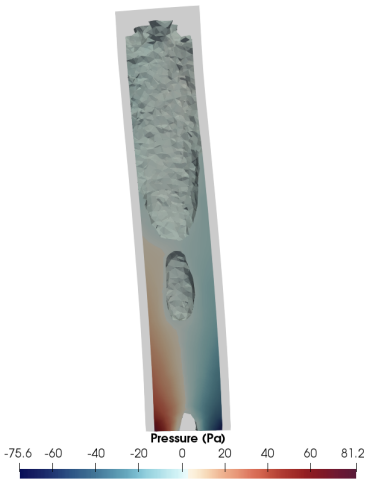

(C) Plane xz. Pressure field

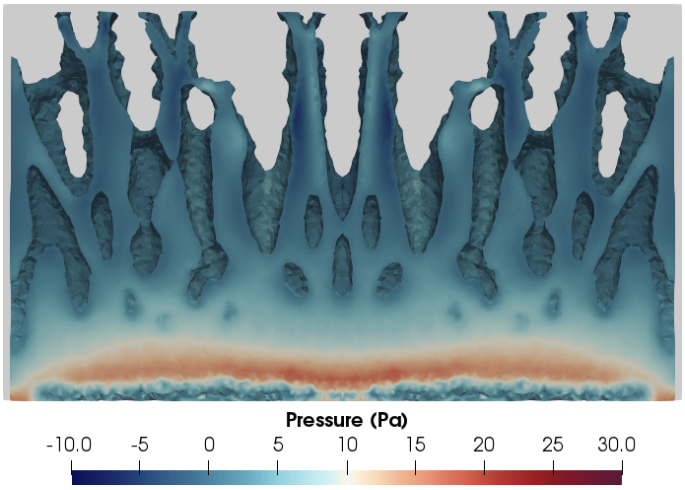

(D) Plane yz. Pressure field

FIGURE 26. Flexible plate in a channel flow. Distribution of the displacement field (top) and pressure (bottom) in the final optimized structures. Displacements are plotted using their Euclidean norm.

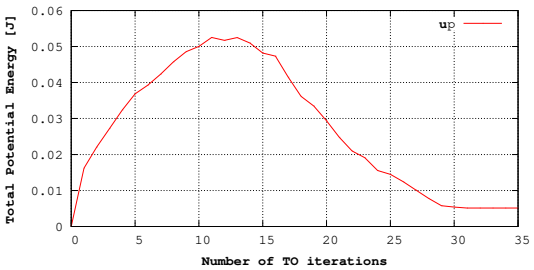

(A) Total potential energy (J)

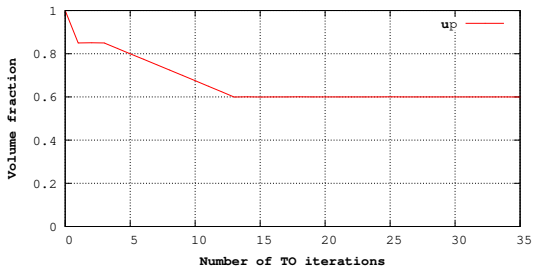

(B) Volume fraction

FIGURE 27. Flexible plate in a channel flow. Convergence curves.

In Section 6 several numerical examples have been shown to assess the performance of the new TO algorithm for incompressible structures subjected to FSI loads. First of all, a

flow through a channel with a flexible wall is considered. This case is supposed to converge to a stationary solution. Several cases have been performed, showing different optimized structures depending upon the kind of solid that is considered and the employed stabilized mixed formulation. The evolution of the total potential energy is also shown to decrease along the TO steps. Next, the well-known Turek's FSI2 test, adapted to the present setting, is performed. The main idea of this problem is to show how the TO algorithm works in transient FSI problems. To do so, several volume fractions for the final structure are considered. Two final transient solutions are obtained for 90% and 80% of the final volume, but a stationary one is achieved when considering a 70% of material. Fluid forces and solid displacements are shown to see the effect of reducing the mass in the beam and how this can modify the physics of the FSI problem. To end up, a 3D case is performed to show the good performance of the methodology in three-dimensional cases.

Acknowledgements

Inocencio Castañar gratefully acknowledges the support received from the Agència de Gestió d'Ajut i de Recerca through the predoctoral FI grant 2019-FI-B-00649. R. Codina gratefully acknowledges the support received through the ICREA Acadèmia Research Program of the Catalan Government. This work was partially funded through the TOP-FSI: RTI2018-098276-B-I00 project of the Spanish Government. CIMNE is a recipient of a "Severo Ochoa Programme for Centers of Excellence in R&D" grant (CEX2018-000797-S) by the Spanish Ministry of Economy and Competitiveness.

Declarations

Conflict of interest. The authors declare that they have no known competing financial interests or personal relationships that could have appeared to influence the work reported in this paper.

Replication of results. All the information required for replicating the paper results was duly presented. Data files for the results are available upon request from the authors.

References

[1] R. Kamakoti and W. Shyy. Fluid-structure interaction for aeroelastic applications. *Progress in Aerospace Sciences*, 40:535–558, 2004.

[2] P.B. Rhyzhakov and E. Oñate. A finite element model for fluid–structure interaction problems involving closed membranes, internal and external fluids. *Computer Methods in Applied Mechanics and Engineering*, 326:422–445, 2017.

[3] T. Bodnár, G. P. Galdi, and S. Nečasová. *Fluid-Structure Interactions and Biomedical Applications*. Springer, 2014. ISBN 978-3-0348-0821-7.

[4] P. Rhyzhakov, E. Soudah, and N. Dialami. Computational modeling of the fluid flow and the flexible intimal flap in type B aortic dissection via a monolithic arbitrary Lagrangian/Eulerian fluid-structure interaction model. *International Journal of Numerical Methods in Biomedical Engineering*, 35:e3239, 2019.

[5] J. Yan, A. Korobenko, X. Deng, and Y. Bazilevs. Computational free-surface fluid–structure interaction with application to floating offshore wind turbines. *Computer and Fluids*, 141:155–174, 2016.

[6] T. Richter and T. Wick. Finite elements for fluid-structure interaction in ALE and fully Eulerian coordinates. *Computer Methods in Applied Mechanics and Engineering*, 199:2633–2642, 2010.

[7] P.B. Rhyzhakov, R. Rossi, S.R. Idelsohn, and E. Oñate. A monolithic Lagrangian approach for fluid–structure interaction problems. *Computational Mechanics*, 46:883–899, 2010.

[8] T. Richter. *Fluid-Structure Interactions*. Springer, 2017. ISBN 978-3-31-963970-7.

[9] U. Küttler and W. A. Wall. Fixed-point fluid–structure interaction solvers with dynamic relaxation. *Computational Mechanics*, 43(1):61–72, 2008.

[10] L. Moreno, I. Castañar, R. Codina, J. Baiges, and D. Cattoni. Numerical simulation of Fluid–Structure Interaction problems with viscoelastic fluids using a log-conformation reformulation. *Computer Methods in Applied Mechanics and Engineering*, 410:115986, 2023.

[11] L.R.G. Treloar. *The Physics of Rubber Elasticity*. Oxford, NY: Oxford University Press, 1975.

[12] E. Comellas, F.J. Bellomo, and S. Oller. A generalized finite-strain damage model for quasi-incompressible hyperelasticity using hybrid formulation. *International Journal for Numerical Methods in Engineering*, 105:781–800, 2016.

[13] J. Martínez-Frutos, R. Ortigosa, and A.J. Gil. In-silico design of electrode meso-architecture for shape morphing dielectric elastomers. *Journal of the Mechanics and Physics of Solids*, 157:104594, 2021.

[14] C. Wex, S. Arndt, A. Stoll, C. Bruns, and Y. Kupriyanova. Isotropic incompressible hyperelastic models for modelling the mechanical behaviour of biological tissues: a review. *Biomedical Engineering*, 60:577–592, 2015.

[15] E. Comellas, T. Gasser, F.J. Bellomo, and S. Oller. A homeostatic-driven turnover remodelling constitutive model for healing in soft tissues. *Journal of the Royal Society Interface*, 13:20151081, 2016.

[16] E. Comellas, S. Budday, J.P. Pelteret, G.A. Holzapfel, and P. Steinmann. Modeling the porous and viscous responses of human brain tissue behavior. *Computer Methods in Applied Mechanics and Engineering*, 369:113128, 2020.

[17] J. Baiges and R. Codina. Variational Multiscale error estimators for solid mechanics adaptive simulations: an Orthogonal Subgrid Scale approach. *Computer Methods in Applied Mechanics and Engineering*, 325:37–55, 2017.

[18] I. Castañar, J. Baiges, and R. Codina. A stabilized mixed finite element approximation for incompressible finite strain solid dynamics using a total Lagrangian formulation. *Computer Methods in Applied Mechanics and Engineering*, 368:113164, 2020.

[19] M. Chiumenti, M. Cervera, and R. Codina. A mixed three-field FE formulation for stress accurate analysis including the incompressible limit. *Computer Methods in Applied Mechanics and Engineering*, 283:1095–1116, 2015.

[20] M. Chiumenti, M. Cervera, C.A. Moreira, and G.B. Barbat. Stress, strain and dissipation accurate 3-field formulation for inelastic isochoric deformation. *Finite Elements in Analysis and Design*, 192:103534, 2021.

[21] I. Castañar, R. Codina, and J. Baiges. A stabilized mixed three-field formulation for stress accurate analysis including the incompressible limit in finite strain solid dynamics. *International Journal for Numerical Methods in Engineering*, 124(10):2341–2366, 2023.

[22] M.P. Bendsøe and O. Sigmund. *Topological Optimization: Theory*. Springer, 2013.

[23] A.A. Novotny and J. Sokolowski. *Topological Derivatives in Shape Optimization*. Springer, 2013.

[24] A.A. Novotny, J. Sokolowski, and A. Zochowski. Topological Derivatives of Shape Functionals. Part I: Theory in Singularly Perturbed Geometrical Domains. *Journal of Optimization Theory and Applications*, 180:341–373, 2019.

[25] M.P. Bendsøe and N. Kikuchi. Generating optimal topologies in structural design using a homogenization method. *Computer Methods in Applied Mechanics and Engineering*, 71(2):197–224, 1988.

[26] X. Huang and Y. Xie. A further review of ESO type methods for topology optimization. *Structural and Multidisciplinary Optimization*, 41:671–683, 2010.

[27] N.P. van Dijk, K. Maute, M. Langelaar, and F. van Keulen. Level-set methods for structural topology optimization: a review. *Structural and Multidisciplinary Optimization*, 48:437–472, 2013.

[28] J.D. Deaton and R.V. Grandhi. A survey of structural and multidisciplinary continuum topology optimization: post 2000. *Structural and Multidisciplinary Optimization*, 49:1–38, 2014.

[29] I. Castañar, J. Baiges, R. Codina, and H. Venghauss. Topological derivative-based topology optimization of incompressible structures using mixed formulations. *Computer Methods in Applied Mechanics and Engineering*, 390:114438, 2022.

[30] R. Ortigosa, J. Martínez-Frutos, A.J. Gil, and D. Herrero-Pérez. A new stabilisation approach for level-set based topology optimisation of hyperelastic materials. *Structural and Multidisciplinary Optimization*, 60:2343–2371, 2019.

[31] R. Ortigosa, D. Ruíz, A.J. Gil, A. Donoso, and J.C. Bellido. A stabilisation approach for topology optimisation of hyperelastic structures with the SIMP method. *Computer Methods in Applied Mechanics and Engineering*, 364:112924, 2020.

[32] Y. Deng, Z. Liu, and Y. Wu. Topology optimization of steady and unsteady incompressible Navier-Stokes flows driven by body forces. *Structural and Multidisciplinary Optimization*, 47(4):555–570, 2013.

[33] L. Shu, M. Y. Wang, and Z. Ma. Level set based topology optimization of vibrating structures for coupled acoustic-structural dynamics. *Computers and Structures*, 132:34–42, 2014.

[34] O.Sigmund and P.M.Clausen. Topology optimization using a mixed formulation: An alternative way to solve pressure load problems. *Computer Methods in Applied Mechanics and Engineering*, 196:1874–1889, 2007.

[35] X. Wang, S. Xu, S. Zhou, W. Xu, M: Leary, P. Choong, M. Qian, M. Brandt, and Y. M. Xie. Topological design and additive manufacturing of porous metals for bone scaffols and orthopaedic implants: a review. *Biomaterials*, 83:127–141, 2016.

[36] C. S. Andreasen and O. Sigmund. Topology optimization of fluid-structure-interaction problems in poroelasticity. *Computer Methods in Applied Mechanics and Engineering*, 258:55–62, 2013.
[37] N. Jenkins and K. Maute. Level set topology optimization of stationary fluid-structure interaction problems. *Structural and Multidisciplinary Optimization*, 52:179–195, 2015.
[38] G. H. Yoon. Topology optimization for stationary fluid-structure interaction problems using a new monolithic formulation. *International Journal of Numerical Methods in Engineering*, 82:591–616, 2010.
[39] G. H. Yoon. Stress-based topology optimization method for steady-state fluid-structure interaction problems. *Computer Methods in Applied Mechanics and Engineering*, 278:499–523, 2014.
[40] N. Jenkins and K. Maute. An immersed boundary approach for shape and topology optimization of stationary fluid-structure interaction problems. *Structural and Multidisciplinary Optimization*, 54:1191–1208, 2016.
[41] R. Picelli, W. M. Vicente, and R. Pavanello. Evolutionary topology optimization for structural compliance minimization considering design-dependent FSI loads. *Finite Elements in Analysis and Design*, 135:44–55, 2017.
[42] F. Feppon, G. Allaire, C. Dapogny, and P. Jolivet. Topology optimization of thermal fluid-structure systems using body-fitted meshes and parallel computing. *Journal of Computational Physics*, 417:109574, 2020.
[43] H. Li, T. Kondoh, P. Jolivet, K. Furuta, T. Yamada, B. Zhu, K. Izui, and S. Nishiwaki. Three-dimensional topology optimization of a fluid-structure system using body-fitted mesh adaption based on the level-set method. *Applied Mathematical Modelling*, 101:276–308, 2022.
[44] Kamilla Emily Santos Silva, Raghavendra Sivapuram, Shahin Ranjbarzadeh, Rafael dos Santos Gioria, Emílio Carlos Nelli Silva, and R Picelli. Topology optimization of stationary fluid–structure interaction problems including large displacements via the TOBS-GT method. *Structural and Multidisciplinary Optimization*, 65(11):337, 2022.
[45] D. Boffi, F. Brezzi, and M. Fortin. *Mixed Finite Element Methods and Applications*. Springer, 2013.
[46] T. J. R. Hughes, G. R. Feijóo, L. Mazzei, and J. Quincy. The variational multiscale method - A paradigm for computational mechanics. *Computer Methods in Applied Mechanics and Engineering*, 166:3–24, 1998.
[47] R.Codina, S.Badia, J.Baiges, and J.Principe. *Variational Multiscale Methods in Computational Fluid Dynamics*. John Wiley & Sons Ltd., 2017.
[48] R. Codina. Stabilization of incompressibility and convection through orthogonal sub-scales in finite element methods. *Computer Methods in Applied Mechanics and Engineering*, 190:1579–1599, 2000.
[49] L. Moreno, R. Codina, J. Baiges, and E. Castillo. Logarithmic conformation reformulation in viscoelastic flow problems approximated by a VMS-type stabilized finite element formulation. *Computer Methods in Applied Mechanics and Engineering*, 354:706–731, 2019.
[50] L. Moreno, R. Codina, and J. Baiges. Solution of transient viscoelastic flow problems approximated by a term-by-term VMS stabilized finite element formulation using time-dependent subgrid-scales. *Computer Methods in Applied Mechanics and Engineering*, 367:113074, 2020.
[51] R. Codina. Finite element approximation of the three field formulation of the Stokes problem using arbitrary interpolations. *SIAM Journal on Numerical Analysis*, 47:699–718, 2009.
[52] J.C. Simo, R.L. Taylor, and K.S. Pister. Variational and projection methods for the volume constraint in finite deformation elasto-plasticity. *Computer Methods in Applied Mechanics and Engineering*, 51(1–3):177–208, 1985.
[53] G. Scovazzi, B. Carnes, X. Zeng, and S. Rossi. A simple, stable, and accurate linear tetrahedral finite element for transient, nearly, and fully incompressible solid dynamics: a dynamic variational multiscale approach. *International Journal For Numerical Methods in Engineering*, 106:799–839, 2016.
[54] G. Chiandussi, G. Bugeda, and E. Oñate. A simple method for automatic update of finite element meshes. *Communications in Numerical Methods in Engineering*, 16:1–19, 1999.
[55] R. Codina. A stabilized finite element method for generalized stationary incompressible flows. *Computer Methods in Applied Mechanics and Engineering*, 190:2681–2706, 2001.
[56] R. Codina, S. Badia, J. Baiges, and J. Principe. Variational Multiscale Methods in Computational Fluid Dynamics. *Encyclopedia of Computational Mechanics, Second Edition*, pages 1–28, 2018.
[57] S. Badia and R. Codina. Analysis of a stabilized finite element approximation of the transient convection-diffusion equation using an ALE framework. *SIAM Journal on Numerical Analysis*, 44:2159–2197, 2006.
[58] R. Codina, J. Principe, and J. Baiges. Subscales on the element boundaries in the variational two-scale finite element method. *Computer Methods in Applied Mechanics and Engineering*, 198:838–852, 2009.
[59] R. Codina, J. Baiges, I. Castañar, I. Martínez-Suárez, L. Moreno, and S. Parada. An embedded strategy for large scale incompressible flow simulations in moving domains. *Journal of Computational Physics*, 488:112181, 2023.

[60] R. Codina and J. Baiges. Finite element approximation of transmission conditions in fluids and solids introducing boundary subgrid scales. *International Journal for Numerical Methods in Engineering*, 87:386–411, 2011.

[61] C.E.L.Pereira and M.L.Bittencourt. Topological sensitivity analysis in large deformation problems. *Structural and Multidisciplinary Optimization*, 37:149–163, 2008.

[62] C.E.L.Pereira and M.L.Bittencourt. Topological sensitivity analysis for a two-parameter Mooney-Rivlin hyperelastic constitutive model. *Latin American Journal of Solids and Structures*, 7:391–411, 2010.

[63] C.G. Lopes, R. Batista dos Santos, and A.A. Novotny. Topological Derivative-based Topology Optimization of Structures Subject to Multiple Load-cases. *Latin American Journal of Solids and Structures*, 12:834–860, 2015.

[64] J. Oliver, D. Yago, J. Cante, and O. Lloberas-Valls. Variational approach to relaxed topological optimization: Closed form solutions for structural problems in a sequential pseudo-time framework. *Computer Methods in Applied Mechanics and Engineering*, 355:779–819, 2019.

[65] D. Yago, J.C. Cante, O. Lloberas-Valls, and J. Oliver. Topology optimization methods for 3d structural problems: a comparative study. *Archives of Computational Methods in Engineering*, 29:1525–1567, 2022.

[66] J. Baiges, J. Martínez-Frutos, D. Herrero-Pérez, F. Otero, and A. Ferrer. Large-scale stochastic topology optimization using adaptive mesh refinement and coarsening through a two-level parallelization scheme. *Computer Methods in Applied Mechanics and Engineering*, 343:186–206, 2019.

[67] T. J. R. Hughes, A. A. Oberai, and L. Mazzei. Large eddy simulation of turbulent channel flows by the variational multiscale method. *Physics of Fluids*, 13:1784–1799, 2001.

[68] R. Codina, J. Principe, and M. Avila. Finite element approximation of turbulent thermally coupled incompressible flows with numerical sub-grid scale modelling. *International Journal of Numerical Methods for Heat & Fluid Flow*, 20:492 – 516, 2010.

[69] O. Colomes, S. Badia, R. Codina, and J. Principe. Assessment of variational multiscale models for the large eddy simulation of turbulent incompressible flows. *Computer Methods in Applied Mechanics and Engineering*, 285:32–63, 2015.

[70] H. A. Van der Vorst. Bi-CGSTAB: A fast and smoothly converging variant of Bi-CG for the solution of nonsymmetric linear systems. *SIAM, Journal of Scientific and Statistical Computing*, 13(2):631 – 644, 1992.

[71] S. Balay, S. Abhyankar, M. F. Adams, J. Brown, P. Brune, K. Buschelman, L. Dalcin, V. Eijkhout, W. D. Gropp, D. Kaushik, M. G. Knepley, D. A. May, L. Curfman McInnes, R. T. Mills, T. Munson, K. Rupp, P. Sanan, B. F. Smith, S. Zampini, H. Zhang, and H. Zhang. PETSc Web page. `http://www.mcs.anl.gov/petsc`, 2015.

[72] S. Turek and J. Hron. Proposal for numerical benchmarking of fluid-structure interaction between an elastic object and laminar incompressible flow. *Fluid–structure interaction. Lecture Notes on Computational Science and Engineering*, pages 371–385, 2007.